Kinetic improvement of an algal diacylglycerol acyltransferase 1 via fusion with an acyl-CoA binding protein

Yang Xu[a], Kristian Mark P. Caldo[a], Lucas Falarz[a,b], Kethmi Jayawardhane[a], Guanqun Chen[a,*]

[a] Department of Agricultural, Food and Nutritional Science, University of Alberta, Edmonton, Alberta, Canada T6G 2P5

[b] Department of Biological Sciences, University of Manitoba, Winnipeg, Manitoba, Canada R3T 2N2

*To whom correspondence should be addressed: Guanqun Chen [Phone: (+1) 780 492-3148; Fax: (+1) 780 492-4265; Email: gc24@ualberta.ca; ORCID: 0000-0001-5790-3903].

ABBREVIATIONS

ACBP, Acyl-CoA binding protein; C16:0, Palmitic acid; C18:0, Stearic acid; C18:1, Oleic acid; C18:2, Linoleic acid; C18:3, α-linolenic acid; DGAT, Diacylglycerol acyltransferase; ER, Endoplasmic reticulum; GPAT, Glycerol-3-phosphate acyltransferase; OD_{600}, Optical density at 600 nm; S.D., Standard derivation; Sc-Ura, Synthetic complete medium lacking uracil; TAG, Triacylglycerol; TLC, Thin-layer chromatography; TMD, Transmembrane domain; WRI, Wrinkled.

SUMMARY

Microalgal oils in the form of triacylglycerols (TAGs) are broadly used as nutritional supplements and biofuels. Diacylglycerol acyltransferase (DGAT) catalyzes the final step of acyl-CoA-dependent biosynthesis of TAG and is considered a key target for manipulating oil production. Although a growing number of *DGAT1*s have been identified and over-expressed in some algal species, the detailed structure-function relationship, as well as the improvement of DGAT1 performance via protein engineering, remain largely untapped. Here, we explored the structure-function features of the hydrophilic N-terminal domain of DGAT1 from the green microalga *Chromochloris zofingiensis* (CzDGAT1). The results indicated that the N-terminal domain of CzDGAT1 was less disordered than those of the higher eukaryotic enzymes and its partial truncation or complete removal could substantially decrease enzyme activity, suggesting its possible role in maintaining enzyme performance. Although the N-terminal domains of animal and plant DGAT1s were previously found to bind acyl-CoAs, replacement of CzDGAT1 N-terminus by an acyl-CoA binding protein (ACBP) could not restore enzyme activity. Interestingly, the fusion of ACBP to the N-terminus of the full-length CzDGAT1 could enhance the enzyme affinity for acyl-CoAs and augment protein accumulation levels, which ultimately drove oil accumulation in yeast cells and tobacco leaves to higher levels than the full-length CzDGAT1. Overall, our findings unravel the distinct features of the N-terminus of algal DGAT1 and provide a strategy to engineer enhanced performance in DGAT1 via protein fusion, which may open a vista in generating improved membrane-bound acyl-CoA-dependent enzymes and boosting oil biosynthesis in plants and oleaginous microorganisms.

KEYWORDS: Triacylglycerol biosynthesis, DGAT, acyl-CoA binding protein, algal lipid, enzyme kinetics, tobacco, yeast, *Chromochloris zofingiensis*

SIGNIFICANCE STATEMENT

Here, we explored the N-terminus of a microalgal DGAT1, a membrane-bound enzyme determining oil biosynthesis, using *in silico* analysis, truncation mutagenesis, protein fusion and *in vitro* and *in vivo* characterization, and demonstrated its distinct structure-function features from the higher eukaryotic enzymes. We further engineered enhanced performance in DGAT1 via N-terminal fusion of ACBP, and obtained a kinetically improved enzyme with augmented protein production levels, which could boost oil accumulation in yeast and plant vegetative tissues.

INTRODUCTION

Plant-derived triacylglycerol (TAG) is one of the most abundant forms of energy storage and reduced carbon in nature, which has been widely used as food, feed and renewable feedstocks for industrial applications (Xu, Caldo, *et al.*, 2018). Microalgae hold the promise of a sustainable bioresource of TAG because of the high ability to accumulate lipids and less competition for arable land with food crops (Xu, Caldo, *et al.*, 2018; Hu *et al.*, 2008). In recent years, the emerging research interest in exploring the oil biosynthesis mechanisms in microalgae has opened an important vista to fulfil the potential of microalgal oil production via physiological and genetic manipulations.

In microalgae, TAG assembly typically occurs through acyl-CoA-dependent and acyl-CoA-independent pathways by a series of acyltransferases which are universally present in plants and animals (Xu, Caldo, *et al.*, 2018; Kong *et al.*, 2018). Among them, acyl-CoA:diacylglycerol acyltransferase (DGAT, EC 2.3.1.20) catalyzes the acylation of *sn*-1,2-diacylglycerol with acyl-CoA to produce TAG, which is the final committed step in the acyl-CoA-dependent TAG biosynthesis. DGAT appears to play a prominent role in affecting the flux of carbon into TAG in many oilseed crops (Liu *et al.*, 2012; Katavic *et al.*, 1995; Zou *et al.*, 1999; Weselake *et al.*, 2008) and has been regarded as an important target for manipulation. Two major forms of membrane-bound non-homologous DGAT, designated DGAT1 and DGAT2, are known to predominantly contribute to TAG formation in developing seeds and microalgae. In plants, DGAT1 is considered as a major player in seed oil accumulation in some oil crops, such as rapeseed (*Brassica napus*) and safflower (*Carthamus tinctorius*) (Rahman *et al.*, 2013; Tzen *et al.*, 1993; Weselake *et al.*, 1993), whereas DGAT2 appears to play a minor role in affecting oil production in oil crops. DGAT2, however, is important for incorporating unusual fatty acids into storage TAG in plants, such as tung tree (*Vernicia fordii*), castor (*Ricinus communis*), and ironweed (*Vernonia galamensis*) (Shockey *et al.*, 2006; Kroon *et al.*, 2006; Li *et al.*, 2010). In microalgae, on the other hand, one or two copies of *DGAT1* and several copies of *DGAT2* were found to likely contribute to the complexity of TAG formation, although their physiological roles remain ambiguous (Mao *et al.*, 2019; Chen and Smith, 2012; Gong *et al.*, 2013; Liu and Benning, 2013; Xu, Caldo, *et al.*, 2018; Turchetto-Zolet *et al.*, 2011; Liu *et al.*, 2016). Given the importance of the enzyme in governing the flux of substrates into TAG, over-expression of *DGAT* cDNAs have been used to manipulate oil production in the seeds of *Arabidopsis thaliana* and oilseed crops

such as soybean (*Glycine max*), *B. napus*, corn (*Zea mays*) and *Camelina sativa* (Jako *et al.*, 2001; Weselake *et al.*, 2008; Roesler *et al.*, 2016; Kim *et al.*, 2016; Oakes *et al.*, 2011; Lardizabal *et al.*, 2008; Li *et al.*, 2012), in the leaves of *Nicotiana tabacum*, *N. benthamiana*, and *Z. mays* (Alameldin *et al.*, 2017; Bouvier-Navé *et al.*, 2000; Vanhercke *et al.*, 2017; Chen *et al.*, 2017), and in oleaginous yeast (Greer *et al.*, 2015; Chen *et al.*, 2017) and several microalgae including *Chlamydomonas reinhardtii*, *Phaeodactylum tricornutum*, and *Nannochloropsis oceanica* (Zulu *et al.*, 2017; Xin *et al.*, 2017; Xin *et al.*, 2018; Mao *et al.*, 2019; Iwai *et al.*, 2014).

DGAT1 is an integral membrane protein with multiple transmembrane domains (TMD), the three-dimensional structure of which has not yet been elucidated (Xu, Caldo, *et al.*, 2018). DGAT1 shares common features among different organisms, containing a very variable hydrophilic N-terminus with possibly distinct functions and a conserved C-terminal region with 8-10 predicted TMD (Liu *et al.*, 2012). The hydrophilic N-termini of *B. napus* and mouse (*Mus musculus*) DGAT1s have been found to be involved in acyl-CoA binding and self-association (Weselake *et al.*, 2006; Siloto *et al.*, 2008; McFie *et al.*, 2010). Recently, the structure of the N-terminal domain of *B. napus* DGAT1 was solved, revealing its important role as an enzyme regulatory domain that positively and negatively modulates enzyme activity (Caldo *et al.*, 2017). The N-terminal domain of *B. napus* DGAT1 consists of two different segments, an intrinsically disordered region encompassing an autoinhibitory motif and a folded segment containing the allosteric site for acyl-CoA and CoA for activation and feedback inhibition of the enzyme, respectively (Caldo *et al.*, 2017). Although DGAT1s have been characterized from a growing number of microalgal species (Kirchner *et al.*, 2016; Wei *et al.*, 2017; Guo *et al.*, 2017; Guihéneuf *et al.*, 2011), the structure-function features of algal DGAT1, as well as using the knowledge in improving DGAT performance, remain largely untapped.

The aim of this study, therefore, is to use a DGAT1 from *Chromochloris zofingiensis* (CzDGAT1), an emerging model green microalgal species for studying TAG and secondary carotenoid accumulation and industrial production, to explore the structure and function features of the N-terminal domain of green microalgal DGAT1 and to investigate the potential of protein fusion in improving DGAT1 performance. After comparing the evolutionary and structural features of algal DGAT1 with the higher eukaryotic enzymes, the function of the hydrophilic N-terminal domain of CzDGAT1 was examined via truncation mutagenesis, protein fusion and *in vitro* enzyme assay. This N-terminus was found to have very different features from those of the

plant and animal enzymes and is important for maintaining high DGAT1 activity but not essential for catalysis. The subsequent fusion of an *A. thaliana* acyl-CoA binding protein (AtACBP6) to the N-terminus of CzDGAT1 resulted in a kinetically improved enzyme with augmented protein production levels, and this improved DGAT1 variant could drive oil accumulation to higher levels than the native DGAT1in yeast cells and *N. benthamiana* leaves. The results indicated the fusion of ACBP with DGAT1 may represents a promising strategy in engineering oil production in oleaginous organisms, which may also be used in engineering other membrane-bound acyl-CoA-dependent enzymes.

RESULTS

CzDGAT1 is phylogenetically related to plant DGAT1

Phylogenetic analysis was carried out with DGAT1s from *C. zofingiensis* and other algae, plants and animals. The two reported full-length *CzDGAT1* sequences, sharing 39.9% amino acid pairwise identity, were both used in this analysis (Roth *et al.*, 2017; Mao *et al.*, 2019). As shown in Figure 1, the results revealed some interesting features from an evolutionary perspective. DGAT1s were found to be separated into four subgroups, with animal and plant DGAT1 falling into two separate groups. DGAT1 from the charophyte green alga *Klebsormidium nitens* is grouped with plant DGAT1, whereas CzDGAT1 and other DGAT1 from chlorophyte green algae form a separate group, which is closely related to the plant DGAT1 group. Diatom DGAT1, on the other hand, is clustered with fungal DGAT1 and is separate from all other sequences.

Further sequence analysis revealed that similar to plant and animal DGAT1s, the C-terminal portion of algal DGAT1s contains 7-10 predicted transmembrane domains and is the most conserved region, whereas the hydrophilic N-terminus preceding the first predicted transmembrane domain is less conserved and variable in length (Figures 1 and S1 and Table S1). Plant and animal DGAT1s have a hydrophilic N-terminus with a length of approximately 110 and 94 amino acid residues, respectively. On the contrary, the N-terminus of the algal DGAT1 has a quite variable length, ranging from 20 (*Chlorella vulgaris* DGAT1) to 326 amino acid residues (*Auxenochlorella protothecoides* DGAT1). One CzDGAT1 isoform (isoform CzDGAT1B in Mao *et al*., 2019) has a N-terminus composed of 107 amino acid residues (Table

S1), which is similar to that of plant and animal DGAT1, and was used for subsequent experiments.

CzDGAT1 encodes an active enzyme and has a hydrophilic N-terminus with less propensity to become disordered

The functionality of CzDGAT1 was characterized using the yeast mutant H1246, which is devoid of TAG biosynthesis ability (Sandager *et al.*, 2002). The yeast complementation and fatty acid feeding assays showed that CzDGAT1 was able to restore TAG biosynthesis in *Saccharomyces cerevisiae* mutant H1246 (Figure 2A) and facilitated the incorporation of the exogenously fed linoleic acid (C18:2$\Delta^{9cis,12cis}$, C18:2) and α-linolenic acid (C18:3$\Delta^{9cis,12cis,15cis}$, C18:3) into yeast TAG (Figure 2B). Further *in vitro* enzyme assay confirmed that CzDGAT1 displayed a strong DGAT activity (Figure 2C).

The N-terminal region of plant DGAT1 has been found to serve important regulatory functions (Caldo *et al.*, 2017). The majority of the N-terminal hydrophilic region of plant and animal DGAT1 is likely present in a disordered state, whereas only a small portion preceding the first predicted transmembrane domain appears to have secondary structure (Figure 2D) (Caldo *et al.*, 2017). To explore whether algal DGAT1 has similar features, the secondary structure of the N-terminal region of algal DGAT1 was analyzed using DISOPRED (Ward *et al.*, 2004). Interestingly, CzDGAT1 may have a very different profile in the N-terminus, where there is much less propensity to be disordered than that of *B. napus* DGAT1 (Figures 2E and F). Similarly, N-terminus with less disordered state was also predicted in DGAT1 from a few other algal species (Figure S2). On the other hand, algal DGAT1 with an extremely long N-terminus, such as DGAT1 from *K. nitens*, is predicted to have both disordered and less disordered N-terminal segments. Furthermore, the folded portion of the N-terminal region of DGAT1 has been found to contain an allosteric site for binding of acyl-CoA and/or CoA has been identified in *B. napus* DGAT1 (Caldo *et al.*, 2017). To test whether the N-terminus of algal DGAT1 also has the regulatory features, the N-terminal regions of DGAT1 from several plants, animal and algal species were aligned (Figure 2D). The four amino acid residues (R96, R97, R99 and E100 in *B. napus* DGAT1) implicated in CoA binding (Caldo *et al.*, 2017) appear to be highly conserved in plant and animal DGAT1 but not in algal DGAT1, in which only the third residue (R99) is

conserved. It should be noted that CzDGAT1 contains partial of the allosteric site in its N-terminus, where two out of the four amino acid residues involved in CoA binding are conserved (Figure 2D).

N-terminal truncation of CzDGAT1 leads to less active enzymes

Considering the partial conservation of the allosteric sites in the N-terminus of CzDGAT1, it is interesting to test whether the N-terminus of CzDGAT1 also serves an analogous function to the *B. napus* DGAT1 N-terminus in catalysis. CzDGAT1 is predicted to have a 107-amino acid residue-long hydrophilic N-terminal region, followed by 9 predicted hydrophobic segments (Figure 3A). To probe the possible role of the N-terminal region, the full-length CzDGAT1 and two N-terminal truncated versions were produced in *S. cerevisiae* mutant H1246 and the microsomal fractions containing the recombinant proteins were used to determine DGAT activity and protein production levels. Both the removal of the first 80 amino acid residues ($CzDGAT1_{81\text{-}550}$), which roughly correspond to the intrinsically disordered region in the N-terminus of *B. napus* DGAT1 (Figure 2D), and the entire N-terminal region ($CzDGAT1_{107\text{-}550}$) led to reduced enzyme production levels (Figure 3B) and enzyme specific activities (Figure 3C). The specific activity of each enzyme was then normalized by the corresponding protein production level and the normalized activities of $CzDGAT1_{81\text{-}550}$ and $CzDGAT1_{107\text{-}550}$ were about 10 and 120-fold lower than that of the full-length enzyme, respectively (Figure 3D). These results suggest that the first 80 amino acids are not dispensable for the enzyme activity, and the entire N-terminal domain may be important for maintaining high enzyme activity.

Fusion with ACBP at the N-terminus of CzDGAT1 and its N-terminal truncation mutant enhanced the enzyme production

The acyl-CoA binding property of the N-terminal region has been revealed in *B. napus* DGAT1 (Weselake *et al.*, 2006; Caldo *et al.*, 2017). Considering the removal of the entire N-terminus of CzDGAT1 led to a nearly inactive enzyme, we further explored whether the N-terminal fusion of $CzDGAT1_{107\text{-}550}$ with an ACBP would restore/improve the enzyme activity. We also tested if the fusion with ACBP could potentially improve DGAT performance by facilitating the channeling of acyl-CoA from the cytosol or the membrane lipid bilayer to the catalytic center of the enzyme.

To test these hypotheses, AtACBP6, a 10-kDa soluble protein, was fused at the N-termini of CzDGAT1, CzDGAT1$_{81-550}$ and CzDGAT1$_{107-550}$, respectively, and the resulting fused proteins were produced in yeast H1246.

As shown in Figure 4A, N-terminal fusion with AtACBP6 largely increased the recombinant protein production in yeast, where the protein accumulation levels of AtACBP6 fused CzDGAT1, CzDGAT1$_{81-550}$ and CzDGAT1$_{107-550}$ were 5, 14, and 28-fold higher than the corresponding unfused CzDGAT1 variants, respectively. The specific activities of the AtACBP6 fused CzDGAT1 and CzDGAT1$_{81-550}$ were also improved to about 2 and 5-fold greater than the unfused enzymes, respectively (Figure 4B). N-terminal fusion of CzDGAT1$_{107-550}$ with AtACBP6, however, led to no improvement in enzyme activity compared to CzDGAT1$_{107-550}$ (Figure 4B). The normalized enzyme activities of AtACBP6 fused CzDGAT1 and CzDGAT1$_{81-550}$ were about 2.5 and 3-fold lower than the unfused enzymes, respectively (Figure 4C), suggesting that the enhanced enzyme activities of the fused proteins were mainly due to the enhanced protein abundance.

N-terminal fusion with ACBP kinetically improves CzDGAT1 and its N-terminal truncation mutant

To further explore the effects of fusing ACBP with DGAT1, the activities of the full-length CzDGAT1, ACBP-fused full-length CzDGAT1, CzDGAT1$_{81-550}$, and ACBP-fused CzDGAT1$_{81-550}$ were analyzed over increasing concentrations of oleoyl-CoA (Figures 5A-D). The full-length enzyme and the N-terminal truncation mutant had a similar response to the increasing acyl-donor concentration, with the maximum enzyme activity achieved at 5 and 7.5 μM oleoyl-CoA, respectively. The ACBP-fused CzDGAT1$_{1-550}$ and CzDGAT1$_{81-550}$, on the other hand, reached the maximum enzyme activity at lower concentrations at 3 and 5 μM oleoyl-CoA, respectively. The substrate saturation curves for CzDGAT1$_{1-550}$ and CzDGAT1$_{81-550}$ and their ACBP-fused versions had better fits to the allosteric sigmoidal equation over the Michaelis-Menten equation (Figures 5A-D). The Hill coefficients of CzDGAT1$_{1-550}$, ACBP-fused CzDGAT1, CzDGAT1$_{81-550}$ and ACBP-fused CzDGAT1$_{81-550}$ were 1.39±0.06, 1.91±0.12, 1.71±0.06, and 1.57±0.14, respectively, which indicates that all these enzymes exhibited positive cooperativity. In addition, CzDGAT1$_{1-550}$ and CzDGAT1$_{81-550}$ had apparent $S_{0.5}$ values of 1.48 ± 0.07 and 1.83 ± 0.05 μM

oleoyl-CoA, respectively (Table 1), suggesting that the oleoyl-CoA affinity of CzDGAT1$_{81\text{-}550}$ might be lower than that of the full-length enzyme. Interestingly, ACBP-fused CzDGAT1$_{1\text{-}550}$ and ACBP-fused CzDGAT1$_{81\text{-}550}$ had apparent $S_{0.5}$ values of 0.94 ± 0.04 and 1.50 ± 0.10 μM oleoyl-CoA, respectively, which are 1.6 and 1.2-fold lower than the values of the corresponding unfused enzymes (Table 1). This result suggests that fusion with ACBP could enhance the affinity of DGAT variants to oleoyl-CoA.

N-terminal fusion with ACBP in CzDGAT1 boosts oil content in yeast and tobacco leaves

In order to determine whether the ACBP fused CzDGAT1 variants can boost oil production to higher levels compared to the native enzyme, cDNAs encoding the full-length CzDGAT1, the N-terminal truncated and the ACBP fused versions were individually introduced into the yeast strain H1246. Expression of *ACBP* or *LacZ* and co-expression of *CzDGAT1$_{1\text{-}550}$* or *CzDGAT1$_{81\text{-}550}$* with *ACBP* in yeast were used as controls. The production of CzDGAT1$_{1\text{-}550}$ led to considerably increased neutral lipid accumulation in yeast at 24 h and 72 h, whereas no change in neutral lipid production was observed for the yeast expressing *CzDGAT1$_{81\text{-}550}$* when compared to the LacZ control (Figure 6A). Fusion with ACBP at the N-terminal of CzDGAT1$_{1\text{-}550}$ but not the N-terminal truncated enzyme was able to further increase the neutral lipid content, resulting in about 2-fold higher production than the native enzyme (Figure 6A). It should be noted that co-expression of *ACBP* with *CzDGAT1$_{1\text{-}550}$* also promoted neutral lipid production in yeast to a comparable level to ACBP-fused CzDGAT1$_{1\text{-}550}$ (Figure 6A), suggesting that ACBP may improve the acyl-CoA availability to DGAT and thus enhance the lipid production.

To further examine the effects of CzDGAT1 variants on oil production in plant vegetative tissues, cDNAs encoding CzDGAT1$_{1\text{-}550}$, ACBP-fused CzDGAT1$_{1\text{-}550}$, CzDGAT1$_{81\text{-}550}$ or ACBP-fused CzDGAT1$_{81\text{-}550}$ were transiently co-expressed with *A. thaliana Wrinkled1* (*AtWRI1*) in the *N. benthamiana* leaves, respectively. *AtWRI1* encodes a transcription factor involved in the upregulation of genes in late glycolysis and fatty-acid biosynthesis (Xu, Caldo, *et al.*, 2018) and co-expression of *AtWRI1* and *DGAT1* was previously found to substantially increase the TAG production in *N. benthamiana* leaves (Vanhercke *et al.*, 2013). The over-expression of a cDNA encoding CzDGAT1$_{1\text{-}550}$ or ACBP-fused CzDGAT1$_{1\text{-}550}$ and the co-expression of *CzDGAT1$_{1\text{-}550}$* and *ACBP* (ACBP + DGAT1$_{1\text{-}550}$) led to considerable increases in

leaf TAG content compared with the expression of *AtWRI1* alone (Figure 6B). Interestingly, ACBP-fused CzDGAT1$_{1-550}$ had a higher impact on improving the leaf TAG production than CzDGAT1$_{1-550}$ or the co-expression group (ACBP + DGAT1$_{1-550}$), where a 1.40 or 1.35-fold increase in TAG content was observed, respectively (Figure 6B). Consistently, the TAG fatty acid composition was also affected in the groups with increased TAG content compared with the *AtWRI1* control group, in which palmitic acid (C16:0) and C18:3 contents were decreased while the content of stearic acid (C18:0), oleic acid (C18:1Δ^{cis9}, C18:1), and C18:2 were increased (Figure 6C). The over-expression of a cDNA encoding ACBP-fused CzDGAT1$_{81-550}$ also resulted in a slight increase in TAG production relative to that of the unfused enzyme, although both groups showed no significant difference in TAG content and composition compared to the *AtWRI1* control group, with an exception of a decrease in C16:0 content in the ACBP-fused CzDGAT1$_{81-550}$ (Figures 6B and C).

To test whether ACBP fusion affects the subcellular localization of CzDGAT1, Venus, a variant of yellow fluorescent protein, was fused to the N-terminal of CzDGAT1$_{1-550}$ or ACBP-CzDGAT1$_{1-550}$, and was transiently co-produced with *A. thaliana* glycerol-3-phosphate acyltransferase (AtGPAT9) containing a C-terminal SCFP3A (a cyan fluorescent protein) fusion in tobacco leaves, which is known to reside in the endoplasmic reticulum (ER) (Gidda *et al.*, 2009). Both CzDGAT1$_{1-550}$ or ACBP-CzDGAT1$_{1-550}$ were found to co-localize with AtGPAT9 (Figure 6D), suggesting their ER localization. It should also be noted that linkage of ACBP to the N-terminus of CzDGAT1 enhanced the CzDGAT1 production in tobacco leaves as indicated by the increased fluorescence intensity (Figure 6E) and enhanced protein accumulation levels based on Western blot analysis (Figures 6F and G).

DISCUSSION

Recently, DGAT1s from a growing number of microalgal species have been characterized with the focus on elucidating their physiological role and application in manipulating oil production (Kirchner *et al.*, 2016; Wei *et al.*, 2017; Guo *et al.*, 2017; Guihéneuf *et al.*, 2011). The structure-function perspectives of algal DGAT1 and the relationship to plant and animal DGAT1, however, remain largely unexplored. In the current study, the evolutionary and structural features of algal DGAT1 in comparison to the higher eukaryotic enzymes were investigated via *in silico* analysis,

truncation mutagenesis and *in vitro* enzyme assay, using DGAT1 of the emerging model green microalga *C. zofingiensis* (Roth *et al.*, 2017; Mao *et al.*, 2019; Liu *et al.*, 2019) as a representative. Moreover, an improved DGAT1 variant was engineered by N-terminal fusion with ACBP, and its potential in enhancing oil production was explored using yeast expression and *N. benthamiana* transient expression systems.

The evolutionary and sequence analyses revealed that CzDGAT1 and other green microalgal DGAT1 are closely related to the plant DGAT1 clade. In addition, algal DGAT1 has similar structural features to plant and animal DGAT1, such as the highly conserved C-terminal hydrophobic region forming multiple TMDs and the variable hydrophilic N-terminal region (Figures 1 and S1 and Table S1). Interestingly, the N-terminus of algal DGAT1 varies dramatically in length ranging from 20 to 326 amino acid residues, which differs from that of plant and animal DGAT1 (Figure 1 and Table S1). The large variation in the N-terminal size appears to be not relevant to the maintenance of enzyme activity, since many DGAT1s with extremely long or short N-termini have been demonstrated to function in TAG biosynthesis (Kirchner *et al.*, 2016; Wei *et al.*, 2017; Mao *et al.*, 2019). Furthermore, the N-terminal region of algal DGAT1 is likely to have different structural features from that of plant and animal DGAT1. The majority of the N-terminus of plant and animal DGAT1 is disordered, while the small folded portion contains a conserved allosteric site (Caldo *et al.*, 2017). On the contrary, the algal DGAT1 N-terminal region has much less propensity to be disordered based on secondary structure analysis (Figures 2E, F and S2) and the possible allosteric site is less conserved in algal DGAT1 (Figure 2D). Taken together, these results suggest that the N-terminal region of algal DGAT1 may have evolved differently from that of plant and animal in terms of structure and function.

The distinct features of the N-terminal domain of algal DGAT1 in enzyme catalysis are also supported by the evidence from the truncation mutagenesis of CzDGAT1. Previous study on *B. napus* DGAT1 suggested that the first 80 amino acid residues in the N-terminal region down regulates enzyme activity and the removal of that region led to higher enzyme activity (Caldo *et al.*, 2017). CzDGAT1 has a N-terminal region (1-107) of a similar size to that of plant and animal DGAT1 (Table S1), but truncation of the equivalent region to the autoinhibitory motif in *B. napus* DGAT1 ($CzDGAT1_{81\text{-}550}$; Figure 2D) diminished the enzyme activity by 10-fold

(Figure 3D), suggesting that this region may not function as an autoinhibitory motif in CzDGAT1. Indeed, the DISOPRED analysis suggested that the N-terminal domain of CzDGAT1 does not have a strong tendency to have the disordered region where autoinhibitory motifs are normally found (Figures 2E and F). Moreover, the N-terminal domain was found to be involved in mediating positive cooperativity in *B. napus* DGAT1, where the N-terminal truncated *B. napus* DGAT1$_{81-501}$ had a decreased Hill coefficient value compared to the full-length enzyme (Caldo *et al.*, 2017). This appears not to be the case for CzDGAT1 since both CzDGAT1 and CzDGAT1$_{81-550}$ exhibited positive cooperativity with close Hill coefficient values (Figures 5A and B, Table 1). Interestingly, N-terminal truncation of CzDGAT1 (CzDGAT1$_{81-550}$) seems to alleviate the substrate inhibition of the full-length enzyme (Figure S3 and Table S2), suggesting that segment 1-80 may be related to a low affinity non-catalytic acyl-CoA binding site. Furthermore, the N-terminal domains of *B. napus* and mouse DGAT1 were shown to be responsible for oligomer formation (McFie *et al.*, 2010; Weselake *et al.*, 2006; Caldo *et al.*, 2017). Although whether this domain functions in self-association in CzDGAT1 remains further exploration, DISOPRED analysis showed that the N-terminus of CzDGAT1 has a less propensity to form protein-protein interactions than *B. napus* and mouse DGAT1 (Figures 2E, F and S2). In addition, truncation of this domain did not affect the self-interaction of CzDGAT1 in the membrane yeast two-hybrid assay (Figure S4). It is also possible that the observed self-interaction was due to the presence of a region in the hydrophobic part of CzDGAT1 that is involved in oligomer formation. Indeed, a 16-kDa fragment of mouse DGAT1 present in the ER lumen was also found to likely form dimer/tetramer (McFie *et al.*, 2010).

The removal of the entire N-terminal region in CzDGAT1 (CzDGAT1$_{107-550}$) almost inactivated the enzyme (Figure 3D), suggesting that the N-terminal region is not necessary for enzyme catalysis but is important for maintaining high enzyme activity. This agrees with the previous studies on the *B. napus* DGAT1 (Caldo *et al.*, 2017). Previously, the N-termini of *B. napus* and mouse DGAT1 were found to associate with acyl-CoA in a sigmoidal fashion (Weselake *et al.*, 2006; Siloto *et al.*, 2008). Replacement of the N-terminal region by ACBP in CzDGAT1 (ACBP fused CzDGAT1$_{107-550}$), however, was not able to restore or improve the enzyme activity (Figure 4), suggesting that the N-terminus may function as a regulatory domain rather than as an acyl-CoA binding site. Indeed, the last 20-30 amino acid residues in the N-terminus of *B. napus* DGAT1 has a well-folded structure and constitutes a regulatory domain for

357 allosteric binding of acyl-CoA and CoA, where the binding of CoA would trigger the subsequent
358 inhibition of DGAT activity (Caldo *et al.*, 2017). The allosteric site for CoA, however, is only
359 partially conserved in CzDGAT1 (Figure 2D), and the activity of CzDGAT1 was not affected in
360 the presence of 50 μM CoA (Figure S5), suggesting that the allosteric site for CoA might be not
361 present in the algal DGAT1 or not activated under this experimental condition. The CoA
362 inhibition was also not triggered by fusion with ACBP to CzDGAT1 (Figure S5), despite that
363 ACBP is able to bind CoA alone (Robinson *et al.*, 1996). However, we cannot rule out the
364 possibility that failure in restoring DGAT activity by replacing the N-terminus with ACBP may
365 be caused by the high binding affinity of ACBP to acyl-CoAs, while a moderate binding affinity
366 being required for the enzyme function. A comprehensive characterization of the N-termini of
367 CzDGAT1 and other algal DGAT1s with respective to the acyl-CoA binding ability would be an
368 interesting next step to explore the possible role of this domain in the catalysis of algal DGATs.

369 The two isoforms of DGAT1 from the green microalga *C. zofingiensis* (Mao *et al.*, 2019)
370 have very distinct features. They share 39.9% amino acid pairwise identity and have very
371 different lengths mainly attributable to the variable N-terminal regions (Figure S1). The N-
372 terminus of the CzDGAT1 isoform studied in the current study is of a similar length to that of
373 plant and animal DGAT1 but with less tendency to be disordered, whereas the other isoform has
374 an extremely long hydrophilic N-terminus of 289 amino acid residues with the first 160 amino
375 acid residues showing low tendency to become disordered and the segment consisting of the
376 remaining 129 residues being highly disordered (Table S1 and Figure S2). Since DGAT1
377 isoform with a longer N-terminus was found to have a higher ability to restore TAG biosynthesis
378 in the yeast mutant (Mao *et al.*, 2019), it is possible that their different N-terminal domain
379 features may directly impact on the enzyme activity and accumulation. Therefore, it would be
380 interesting to comprehensively compare the structure and function features of the N-terminal
381 domains of both CzDGAT1 isoforms in the future. Additionally, it may also be worthwhile to
382 explore the activities and physiological functions of CzDGAT1 in detail, especially considering
383 that the coding genes of both isoforms were up-regulated under nitrogen deprivation and high-
384 light stress conditions to contribute to TAG accumulation but with very different transcript
385 abundances (under both conditions) and response patterns (under high-light stress) (Roth *et al.*,
386 2017; Mao *et al.*, 2019; Liu *et al.*, 2019).

It is interesting to note that N-terminal fusion with ACBP could markedly increase the yeast recombinant protein production up to 28 folds (Figure 4A). It has been suggested that the identity of the amino acid residues at the N-terminus of proteins could potentially affect the protein turnover and/or translation rate and thus enhance the protein production (Greer *et al.*, 2015; Sriram *et al.*, 2011). Indeed, the addition of N-terminal tag was found to increase the production of *B. napus* DGAT1 and plant fatty acid desaturases in yeast cells (O'Quin *et al.*, 2009; Greer *et al.*, 2015). Previously, fusion with small soluble proteins, such as thioredoxin, ubiquitin and maltose binding protein was also found to augment the accumulation levels of recombinant protein in *Escherichia coli* and/or yeast likely by improving protein stability and/or translation efficiency (Marsh *et al.*, 1989; Pryor and Leiting, 1997; Jacquet *et al.*, 1999; Ecker *et al.*, 1989). The protein fusion strategy, especially fusion to ubiquitin, has also met considerable success in increasing protein production in transgenic plants (Mishra *et al.*, 2006; Tian and Sun, 2011; Hondred *et al.*, 1999; Streatfield, 2007). Our finding that linkage to ACBP enhanced the CzDGAT1 production in tobacco leaves (Figures 6E-G) suggests that ACBP might also have potential to be used as a protein fusion partner to enhance protein accumulation in plants, especially for membrane-bound acyl-CoA-dependent enzymes.

Fusion with ACBP not only augmented the production of CzDGAT1 (Figures 4A and 6E-G) but also improved the kinetic parameters of the enzyme (Figure 5). Our kinetic analysis showed that ACBP-fused CzDGAT1$_{1\text{-}550}$ or ACBP-fused CzDGAT1$_{81\text{-}550}$ still exhibited positive cooperativity despite that ACBP binds acyl-CoA in a typical hyperbolic manner (Brown *et al.*, 1998; Yurchenko *et al.*, 2009) and, more importantly, the fused enzymes had increased affinity for oleoyl-CoA with the apparent $S_{0.5}$ values decreasing by 1.6 and 1.2-fold, respectively (Table 1 and Figure 5). DGAT affinity for oleoyl-CoA has been reported as an important determinant of oil production since a strong correlation of oleoyl-CoA affinity with oil content was found in soybean expressing *DGAT1* variants (Roesler *et al.*, 2016). Cytosolic 10-kDa ACBP, consisting of four α helixes (Figure S6), is capable of binding acyl-CoAs with high affinity (Robinson *et al.*, 1996; Du *et al.*, 2016). Considering the increased DGAT affinity for oleoyl-CoA of the ACBP-fused CzDGAT1, we proposed that ACBP would facilitate the feeding of acyl-CoA to the catalytic pocket of CzDGAT1 via capturing cytosolic acyl-CoAs (or those partitioned into the membrane lipid bilayer) and subsequent channeling to DGAT by proximity (Figure S6). Similarly, fusion of proteins in a consecutive reaction has been shown to have synergistic effects

in substrate conversion in a single catalytic region (Elleuche, 2015). ACBP has been implicated in acyl-CoA binding and transport, which maintains the substrate supply for the acyl-CoA-dependent acyltransferases in the ER, including DGAT (Yurchenko and Weselake, 2011). Recently, ACBP2 was found to probably interact directly with lysophospholipase 2 in *A. thaliana* and thereby facilitate the lysophosphatidylcholine hydrolysis (Miao *et al.*, 2019). Therefore, it is plausible to assume the presence of transient interactions between ACBP and DGAT, the enhancement of which via protein fusion may further lead to an efficient substrate channeling. Furthermore, *B. napus* ACBP has been shown to slightly stimulate DGAT1 activity when the concentration of acyl-CoA is higher than that of ACBP, but to inhibit DGAT activity when ACBP is in excess likely due to the competition of ACBP with ACBP-bound acyl-CoA or DGAT for enzyme-substrate interaction (Yurchenko and Weselake, 2011). ACBP-fused CzDGAT1 or CzDGAT1$_{81\text{-}550}$, on the other hand, showed a more rapid response to increasing acyl-CoA concentration from 0.1 to 5 or 10 µM than the unfused enzymes, respectively (Figure 5 and Table 1), suggesting that in the 1:1 fusion form ACBP may facilitate enzyme-substrate binding rather than compete with DGAT for substrate.

The kinetically improved DGAT1 via fusion with ACBP shows promises in oil production in both yeast and plant systems (Figure 6). Although ACBP-fused DGAT1 was able to augment the yeast neutral lipid production up to two-fold relative to that of the unfused enzyme, a comparable level was also achieved in the yeast co-expressing individual fusion groups (Figure 6A). In tobacco transient expression system, ACBP-fused DGAT1 was more efficient to boost leaf TAG content than the unfused enzyme and the co-expressed group. It should be noted that the sizes of the acyl-CoA pool in yeast and tobacco leaf cells are different. The cellular concentration of total acyl-CoA pool in *S. cerevisiae* has been reported to be in the range of 10-42 µM depending on the strain and its metabolic state (Schjerling *et al.*, 1996; Mandrup *et al.*, 1993; Knudsen *et al.*, 1994); whereas the concentration of total acyl-CoAs in tobacco leaves was determined to be 0.5 µM (Moreno *et al.*, 2014) [intracellular concentrations were converted to µM assuming a specific cell volume of 3.7×10^{-14} L/cell (Krink-Koutsoubelis *et al.*, 2018) and 1 mg equal to 1 µL volume (Larson and Graham, 2001), for yeast and plant cells, respectively]. Co-production of ACBP and DGAT1 appears to work better in the cells with the acyl-CoA concentration at higher levels rather than lower levels (Figures 6A and B). It is possible that co-production of ACBP with DGAT1 affected *in vivo* DGAT1 activity in a manner

dependent on the cellular acyl-CoA concentration, where co-produced ACBP stimulates DGAT1 activity at high acyl-CoA concentration but restricts DGAT1 activity at low acyl-CoA concentration, which agrees with the previous finding on the *in vitro* stimulation of DGAT activity by *B. napus* ACBP (Yurchenko and Weselake, 2011). ACBP-fused DGAT1, on the other hand, showed good performance in cells with both low and high concentrations of acyl-CoAs (Figures 6A and B) likely due to the improved enzyme kinetics and protein production levels, despite that fusion with ACBP slightly enhanced the substrate inhibition of DGAT1 at the acyl-CoA concentrations above 10 μM (Figure S3 and Table S2). Moreover, it would be interesting to explore the potential of co-producing DGAT with other ACBP isoforms, such as ER-bound ACBP, in improving TAG production, since both soluble and ER-bound ACBP may be involved in the capture and shuttle of acyl-CoAs for downstream acyl-CoA-dependent acyltransferases.

In conclusion, our results suggested that algal DGAT1 may have different evolutionary and structural features from plant and animal DGAT1 with respect to the hydrophilic N-terminal domain. This domain is predicted to be present in a less disordered state in CzDGAT1 than that of animal/plant DGAT1. Although the N-terminal domain is not necessary for acyltransferase activity of CzDGAT1, its removal, however, led to huge decreases in CzDGAT1 enzyme activity, which cannot be restored by fusion with an ACBP. We also found that fusion of ACBP to the N-terminus of the full-length CzDGAT1 could not only augment the protein accumulation levels in yeast and tobacco leaves but also kinetically improve the enzyme. ACBP-fused DGAT1 was more effective in improving the oil contents of yeast cells and vegetative tissues than the native DGAT1. This strategy may have great potential in engineering membrane-bound acyl-CoA-dependent enzymes and manipulating oil biosynthesis in plants, algae and other oleaginous organisms.

EXPERIMENTAL PROCEDURES

Sequence analysis

Multiple sequence alignments of DGAT1 proteins from different animal, plant and microalgal species (Table S1) were performed using the L-INS-i method implemented in MAFFT v7.271 (Katoh and Standley, 2013) and trimmed using trimAl v1.2 (Capella-Gutiérrez *et al.*, 2009). The

478 resulting alignments were used for model selection using IQ-TREE (v1.3.11.1) with the option "-
479 m TESTONLY". The phylogenetic tree was then constructed with the best-fit model for protein
480 alignment (LG+F+I+G) using Phyml v3.0 (Guindon *et al.*, 2010) and visualized with iTOL v3
481 (Letunic and Bork, 2016). The topology organization of DGAT1 was predicted using TMHMM
482 (Krogh *et al.*, 2001).

483

484 **Construct preparation, yeast transformation and heterologous expression of *DGAT1***
485 **variants**

486 The coding sequence of *CzDGAT1* (Phytozome accession number: Cz09g08290) was chemically
487 synthesized (General Biosystems, Morrisville, NC), and re-cloned into the pYES2.1 yeast
488 expression vector (Invitrogen, Burlington, Canada) under the control of the galactose-inducible
489 *GAL1* promoter. N-terminal truncation mutants of *CzDGAT1* were PCR-amplified and subcloned
490 into the pYES2.1 vector. The coding sequence of *AtACBP6* (NCBI accession number:
491 NM_102916) was PCR-amplified from the plasmid pAT332 (kindly provided by Dr. Mee-Len
492 Chye, University of Hong Kong) (Chen *et al.*, 2008), and subcloned into the pYES2.1 vector and
493 the pESC-leu2d(empty) vector (a gift from Dr. Jay Keasling; Addgene plasmid # 20120) (Ro *et*
494 *al.*, 2006). To generate ACBP-CzDGAT1$_{1\text{-}550}$, ACBP-CzDGAT1$_{81\text{-}550}$ and ACBP-CzDGAT1$_{107\text{-}550}$ fusion proteins, the coding sequences of *AtACBP6* and variant *CzDGAT1s* were individually
496 amplified and the resulting amplicons were fused using overlap extension PCR. The DNA
497 sequences of ACBP-CzDGAT1$_{1\text{-}550}$, ACBP-CzDGAT1$_{81\text{-}550}$ and ACBP-CzDGAT1$_{107\text{-}550}$ fusion
498 proteins were then subcloned into the pYES2.1 vector. The stop codon was removed from each
499 sequence for in-frame fusion with a C-terminal V5 tag, which is encoded in the pYES2.1 vector.
500 The primers used for the preparation of all the constructs are listed in Table S3.

501 After the integrity of each construct was confirmed by sequencing, the constructs were
502 transformed into the quadruple mutant strain *S. cerevisiae* H1246 (*MATα are1-Δ::HIS3, are2-*
503 *Δ::LEU2, dga1-Δ::KanMX4, lro1-Δ::TRP1 ADE2*) using an *S.c.* EasyComp Transformation Kit
504 (Invitrogen) for yeast heterologous expression (Xu, Holic, *et al.*, 2018; Xu *et al.*, 2017; Xu *et al.*,
505 2019). The recombinant yeast cells were first cultured overnight in liquid minimal medium
506 containing 0.67% (w/v) yeast nitrogen base, 0.2% (w/v) synthetic complete medium lacking
507 uracil (SC-Ura) and 2% (w/v) raffinose. The yeast cultures were then used to inoculate the

induction medium containing 0.67% (w/v) yeast nitrogen base, 0.2% (w/v) SC-Ura, 2% (w/v) galactose, and 1% (w/ v) raffinose at an initial optical density of 0.4 at 600 nm (OD_{600}). For co-expression of *AtACBP6* and *CzDGAT1*, SC-Ura in the liquid minimal medium was replaced by synthetic complete medium lacking leucine and uracil. For the fatty acid feeding experiment, yeast cells were cultured in the induction medium with the supplementation of 200 mM of C18:2 or C18:3 fatty acid. Yeast cultures were grown at 30^{o}C with shaking at 220 rpm.

Preparation of yeast microsomal fractions

Microsomal fractions containing recombinant CzDGAT1 variants were isolated from yeast cells as described previously (Xu *et al.*, 2017; Xu *et al.*, 2019; Xu, Holic, *et al.*, 2018). In brief, the recombinant yeast cells were collected at the mid log growth stage with an OD600 value around 6.5, washed, and then resuspended in 1 mL of lysis buffer [20 mM Tris-HCl pH 7.9, containing 10 mM $MgCl_2$, 1 mM EDTA, 5% (v/v) glycerol, 300 mM ammonium sulfate and 2 mM dithiothreitol]. The cells were homogenized by a bead beater (Biospec, Bartlesville, OK, USA) in the presence of 0.5 mm glass beads and then centrifuged at 10 000 g at 4^{o}C for 30 min to remove cell debris and glass beads. The recovered supernatant was further centrifuged at 105 000 g at 4^{o}C for 70 min to pellet the microsomes. The resulting microsomal fractions were resuspended in ice-cold suspension buffer (3 mM imidazole buffer, pH 7.4, and 125 mM sucrose). Protein concentration was quantified by the Bradford assay (Bio-Rad, Mississauga, Canada) using BSA as a standard (Bradford, 1976).

***In vitro* DGAT1 assay**

In vitro DGAT assay was performed according to the procedure described previously (Xu *et al.*, 2017; Xu *et al.*, 2019; Xu, Holic, *et al.*, 2018). Briefly, a 60-μL reaction mixture containing 200 mM HEPES-NaOH (pH 7.4), 3.2 mM $MgCl_2$, 333 μM *sn*-1,2-diolein [dispersed in 0.2% (v/v) Tween 20], 15 μM [1-^{14}C] oleoyl-CoA (56 μCi/μmol; American Radiolabeled Chemicals, St. Louis, MO, USA), and 10-50 μg of microsomal protein was incubated at 30^{o}C for 4-30 min with shaking. The reaction was initiated by adding microsomes containing recombinant CzDGAT1 variants and terminated by adding 10 μL of 10% (w/v) SDS. The entire reaction mixture was

then loaded onto a thin-layer chromatography (TLC) plate (0.25 mm Silica gel, DC-Fertigplatten, Macherey-Nagel, Germany). The plate was developed with hexane/diethyl ether/acetic acid (80:20:1, v/v/v) and the resolved lipids were visualized by phosphorimaging (Typhoon Trio Variable Mode Imager, GE Healthcare, Mississauga, Canada). The corresponding TAG spots were scraped and quantified for radioactivity using a LS 6500 multi-purpose scintillation counter (Beckman-Coulter, Mississauga, Canada).

For kinetic assay, the concentration of [1-^{14}C] oleoyl-CoA was varied from 0.1 to 25 μM while *sn*-1,2-diolein was held constant at 333 μM. The DGAT assay reaction time and the quantity of microsomal protein used were as follows: for CzDGAT1$_{1\text{-}550}$ and ACBP-CzDGAT1$_{1\text{-}550}$, 10 μg of microsomal protein for 4 min; for ACBP-CzDGAT1$_{81\text{-}550}$, 5 μg of microsomal protein for 30 min; for CzDGAT1$_{81\text{-}550}$, 10 μg of microsomal protein for 30 min. Enzyme kinetic parameters were calculated by fitting the data to the Michaelis-Menten equation, allosteric sigmoidal equation, or a previously proposed model accounting for sigmoidicity and substrate inhibition (Xu *et al.*, 2017) using the program GraphPad Prism (version 6.0; GraphPad Software, La Jolla, CA, USA).

Transient expression of *CzDGAT1* variants in *N. benthamiana* leaves

N. benthamiana plants were grown in a growth chamber at 25°C, 50% humidity and 16/8 hr day/night cycle. For transient expression in *N. benthamiana* leaves for lipid production, cDNAs encoding *AtWRI1* (previously isolated using *A. thaliana* cDNA in our lab), CzDGAT1$_{1\text{-}550}$, the N-terminal truncation mutant (CzDGAT1$_{81\text{-}550}$) and their ACBP-fused versions (ACBP-CzDGAT1$_{1\text{-}550}$ and ACBP-CzDGAT1$_{81\text{-}550}$) were subcloned in a pGREEN 0229 vector under a *cauliflower mosaic virus* (*CaMV*) *35S* promoter, respectively. For the examination of the subcellular localization, cDNAs encoding CzDGAT1$_{1\text{-}550}$ and ACBP-CzDGAT1$_{1\text{-}550}$ were fused in frame to the downstream of *Venus*, which was amplified from the pSYFP2-SCFP3A plasmid (a gift from Dr. Dorus Gadella; Addgene plasmid # 22905) (Kremers *et al.*, 2006), and was inserted downstream of a *CaMV 35S* promoter in the modified pGPTVII vector (kindly provided by Dr. Jörg Kudla, University of Münster) (Becker *et al.*, 1992; Gehl *et al.*, 2009). The coding sequence of *AtGPAT9* (Singer *et al.*, 2016) was fused in frame to the upstream of *SCFP3A*

(amplified from the pSYFP2-SCFP3A plasmid), subcloned in the modified pGPTVII vector under a *CaMV 35S* promoter and used as an ER marker (Gidda *et al.*, 2009).

All constructs were individually transformed to *Agrobacterium tumefaciens* GV3101 cells via electroporation. Each pGREEN construct was transformed along with the pSOUP helper plasmid. *A. tumefaciens* cultures containing the *p19* vector encoding a viral suppressor protein and each variant *CzDGAT1* were mixed in a transformation medium [50 mM MES, 2 mM Na_3PO_4, 0.5% (w/v) glucose and 0.1 mM acetosyringone] with the final OD_{600} of each culture equal to 0.125 (or 0.25 for subcellular localization experiments) prior to infiltration into *N. benthamiana* leaves as described by Vanhercke et al. (2013). For lipid analysis, *N. benthamiana* plants were grown for a further five days before leaf samples were collected, flash frozen, freeze-dried, and stored at -80°C. For protein extraction, *N. benthamiana* leaves were harvested after 2 days of infiltration and were ground in liquid nitrogen to a fine powder using mortar and pestle. The resulting leaf powders were then mixed with 1 volume (v/w) of ice-cold extraction buffer (4 M urea, 100 mM DTT, 1% Triton X-100, and 1 mM PMSF), and incubated on ice for 10 min. The homogenate was clarified by centrifugation at 12 000 g for 5 min at 4°C and the supernatant was used for SDS-PAGE gel analysis immediately after preparation.

For subcellular localization experiments, *AtGPAT9-SCFP3C* was co-infiltrated with the *p19* vector and *Venus-CzDGAT1* or *Venus-ACBP-CzDGAT1* and the fluorescence of the lower epidermis of leaves after 2-3 days of infiltration was visualized using a fluorescent microscope (Axio Imager M1m microscope; Carl Zeiss Inc., Germany). The excitation wavelengths for Venus and SCFP3A were 546/12 and 365 nm, respectively, and the emission filter wavelengths were 575–640 nm for Venus and 455/50 nm for SCFP3A. For the quantification of fluorescence intensity, the fluorescent proteins were extracted from tobacco leaves transiently expressing the *p19* vector and *Venus-CzDGAT1* or *Venus-ACBP-CzDGAT1* by grinding on ice with a two-fold volume of pre-chilled extraction buffer containing 100 mM MOPS (pH 7.2), 5 mM $MgCl_2$, 0.02% BSA and 1% protease inhibitor, followed by centrifugation. One hundred microliters of the supernatant were then placed into 96-well solid black plates (Corning Inc., Corning, NY, USA) and the fluorescence intensity of Venus-tagged protein was measured on a Synergy H4 Hybrid reader (Biotek, Winooskit, VT, USA) at excitation and emission wavelengths of 485 nm and 528 nm, respectively.

596 **Western blotting**

597 Equivalent amounts of yeast microsomal proteins (15 μg) or protein extracts from leaf samples
598 containing recombinant CzDGAT1 variants were incubated with 5× SDS loading buffer at room
599 temperature for 15 min, resolved through SDS-PAGE Gels (Bio-Rad) and electrotransfered (2 h
600 at 80 V or 16 h at 30 V and 4^{o}C) onto polyvinylidene difluoride membrane (Amersham, GE
601 Healthcare). The recombinant enzymes were probed using anti-V5-HRP conjugated antibody
602 (Invitrogen), which was detected using an ECL Advance Western Blotting Detection Kit
603 (Amersham) by a FluorChem SP imager (Alpha Innotech Corp., San Leandro, CA, U.S.A.). The
604 band densities were semi-quantified with ImageJ software (Schneider *et al.*, 2012).

605

606 **Lipid analysis**

607 The yeast neutral lipid content was analyzed by the Nile red fluorescence assay as described
608 previously (Xu *et al.*, 2017). In brief, an aliquot (100 μL) of yeast culture was incubated with 5
609 μL of Nile red solution (0.1 mg/mL in methanol) into 96-well solid black plates (Corning Inc.).
610 The fluorescence was measured before and after the addition of the Nile red solution with
611 excitation and emission at 485 and 538 nm, respectively, using a Synergy H4 Hybrid reader
612 (Biotek). The neutral lipid content in yeast was represented by the Nile red values which were
613 calculated based on the change in fluorescence over OD_{600} ($\Delta F/OD_{600}$).

614 The TAG content and fatty acid composition of yeast cells and *N. benthamiana* leaf
615 samples were analyzed using GC/MS. Yeast total lipids were extracted from approximately 30
616 mg of lyophilized yeast cells as described previously (Xu *et al.*, 2019; Xu, Holic, *et al.*, 2018).
617 As for *N. benthamiana* leaf samples, 70 mg lyophilized leaf tissues were homogenized in
618 chloroform: isopropanol (2:1, v/v) for total lipids extraction as described previously
619 (Mietkiewska *et al.*, 2014). For quantification, 100 μg of triheptadecanoin (C17:0 TAG) were
620 added to each sample as an internal standard. The extracted lipids were further separated on a
621 TLC plate (0.25 mm Silica gel, DC-Fertigplatten) as described above and the lipid bands were
622 visualized by spraying with primulin solution [0.05% primulin (w/v) in acetone/water (80:20,
623 v/v)]. The corresponding TAG bands were then scraped and trans-methylated by incubating with
624 1 mL of 3 N methanolic HCl at 80 °C for 1 h. The resulting fatty acid methyl esters were
625 analyzed using GC/MS (Agilent Technologies, Wilmington, DE) equipped with a capillary DB-

626 23 column (30 m × 0.25 mm × 0.25 μm) as described previously (Xu *et al.*, 2019; Xu, Holic, *et*
627 *al.*, 2018).

628

629 **Statistical analysis**

630 Data are shown as means ± standard derivation (S.D.) for the number of independent
631 experiments indicated. Significant differences between two groups were assessed using a
632 Student's t-test with the SPSS statistical package (SPSS 16.0, Chicago, IL, USA). The equality
633 of variance was tested by Levene's test. The unpaired Student's t-test assuming equal variances
634 and the unpaired Student's t-test with Welch corrections assuming unequal variances were
635 performed when the variances were equal and unequal, respectively.

636

637 **ACCESSION NUMBERS**

638 Sequence data from this article can be accessed in the Phytozome/GenBank/Arabidopsis
639 Genome Initiative databases under the following accession numbers: AtACBP6, NM_102916;
640 AtGPAT9, AT5G60620; AtWRI1, AY254038; CzDGAT1, Cz09g08290.

641

642 **ACKNOWLEDGEMENTS**

643 We acknowledge the support provided by the University of Alberta Start-up Research Grant,
644 Natural Sciences and Engineering Research Council of Canada Discovery Grant (RGPIN-2016-
645 05926) and the Canada Research Chairs Program. We are grateful to Dr. Mee-Len Chye
646 (University of Hong Kong) for providing the plasmid pAT332 containing the coding sequence of
647 *AtACBP6* and Dr. Igor Stagljar (University of Toronto) for providing the membrane yeast two-
648 hybrid system. We also thank Dr. Stacy Singer (Agriculture and Agri-Food Canada) for sharing
649 her experience on tobacco leaf infiltration, Dr. Michael Gänzle, Dr. Yuan Fang and Mr. Kosala
650 Waduthanthri (University of Alberta) for their assistance in fluorescence microscopy and Dr.
651 Shanjida Khan (University of Alberta) for providing the *N. benthamiana* seeds.

652

653

AUTHOR CONTRIBUTIONS

GC supervised the experiment; YX, GC, and KMPC designed the experiment; YX performed the experiments and prepared the initial draft of the manuscript. YX, KMPC and LF analyzed the data. KMPC and KJ contributed valuable discussion during this study. All authors were involved in further editing of the manuscript.

CONFLICT OF INTEREST

The authors declare that they have no conflicts of interest with the content of this article.

SUPPORTING INFORMATION

Method S1. Membrane yeast two-hybrid assay.

Table S1. DGAT1 proteins used for multiple sequence alignment.

Table S2. Apparent kinetic parameters of CzDGAT1 variants using a combined model accounting for sigmoidicity and substrate inhibition (Xu et al., 2017).

Table S3. Primers used in the current study.

Figure S1. Alignment of DGAT1 from different species.

Figure S2. Prediction of intrinsic disorder profile (blue) of the N-terminal region of DGAT1 from representative algae, plant and animals and its likelihood to participate in protein-protein interaction (red).

Figure S3. DGAT activity of CzDGAT1 variant enzymes at high oleoyl-CoA concentrations.

Figure S4. Probing possible self-interaction of CzDGAT1 variants using membrane yeast two-hybrid assay.

Figure S5. Enzyme activity of CzDGAT1 variants in the presence of Coenzyme A (CoA).

Figure S6. Illustration of the N-terminal fusion of acyl-CoA binding protein (ACBP) to CzDGAT1.

REFERENCES:

Alameldin, H., Izadi-Darbandi, A., Smith, S.A. and Balan, V. (2017) Metabolic engineering to increase the corn seed storage lipid quantity and change its compositional quality. *Crop Sci*, **57**, 1854–1864.

Becker, D., Kemper, E., Schell, J. and Masterson, R. (1992) New plant binary vectors with selectable markers located proximal to the left T-DNA border. *Plant Mol. Biol.*, **20**, 1195–1197.

Bouvier-Navé, P., Benveniste, P., Oelkers, P., Sturley, S.L. and Schaller, H. (2000) Expression in yeast and tobacco of plant cDNAs encoding acyl CoA:diacylglycerol acyltransferase. *FEBS J.*, **267**, 85–96.

Bradford, M.M. (1976) A rapid and sensitive method for the quantitation of microgram quantities of protein utilizing the principle of protein-dye binding. *Anal. Biochem.*, **72**, 248–254.

Brown, A.P., Johnson, P., Rawsthorne, S. and Hills, M.J. (1998) Expression and properties of acyl-CoA binding protein from *Brassica napus*. *Plant Physiol. Biochem.*, **36**, 629–635.

Caldo, K.M.P., Acedo, J.Z., Panigrahi, R., et al. (2017) Diacylglycerol acyltransferase 1 is regulated by its N-terminal domain in response to allosteric effectors. *Plant Physiol*, **175**, 667–680.

Capella-Gutiérrez, S., Silla-Martínez, J.M. and Gabaldón, T. (2009) trimAl: A tool for automated alignment trimming in large-scale phylogenetic analyses. *Bioinformatics*, **25**, 1972–1973.

Chen, G., Xu, Y., Siloto, R.M.P., et al. (2017) High-performance variants of plant diacylglycerol acyltransferase 1 generated by directed evolution provide insights into structure function. *Plant J*, **92**, 167–177.

Chen, J.E. and Smith, A.G. (2012) A look at diacylglycerol acyltransferases (DGATs) in algae. *J. Biotechnol.*, **162**, 28–39.

Chen, Q.-F., Xiao, S. and Chye, M.-L. (2008) Overexpression of the Arabidopsis 10-kilodalton acyl-Coenzyme A-binding protein ACBP6 enhances freezing tolerance. *Plant Physiol.*, **148**,

304–315.

Du, Z.Y., Arias, T., Meng, W. and Chye, M.L. (2016) Plant acyl-CoA-binding proteins: An emerging family involved in plant development and stress responses. *Prog. Lipid Res.*, **63**, 165–181.

Ecker, D.J., Stadel, J.M., Butt, T.R., et al. (1989) Increasing gene expression in yeast by fusion to ubiquitin. *J. Biol. Chem.*, **264**, 7715–7719.

Elleuche, S. (2015) Bringing functions together with fusion enzymes—from nature's inventions to biotechnological applications. *Appl. Microbiol. Biotechnol.*, **99**, 1545–1556.

Gehl, C., Waadt, R., Kudla, J., Mendel, R.R. and Hänsch, R. (2009) New GATEWAY vectors for high throughput analyses of protein-protein interactions by bimolecular fluorescence complementation. *Mol. Plant*, **2**, 1051–1058.

Gidda, S.K., Shockey, J.M., Rothstein, S.J., Dyer, J.M. and Mullen, R.T. (2009) *Arabidopsis thaliana* GPAT8 and GPAT9 are localized to the ER and possess distinct ER retrieval signals: Functional divergence of the dilysine ER retrieval motif in plant cells. *Plant Physiol. Biochem.*, **47**, 867–879.

Gong, Y., Zhang, J., Guo, X., Wan, X., Liang, Z., Hu, C.J. and Jiang, M. (2013) Identification and characterization of PtDGAT2B, an acyltransferase of the DGAT2 acyl-Coenzyme A: Diacylglycerol acyltransferase family in the diatom *Phaeodactylum tricornutum*. *FEBS Lett.*, **587**, 481–487.

Greer, M.S., Truksa, M., Deng, W., Lung, S.C., Chen, G. and Weselake, R.J. (2015) Engineering increased triacylglycerol accumulation in *Saccharomyces cerevisiae* using a modified type 1 plant diacylglycerol acyltransferase. *Appl. Microbiol. Biotechnol.*, **99**, 2243–2253.

Guihéneuf, F., Leu, S., Zarka, A., et al. (2011) Cloning and molecular characterization of a novel acyl-CoA:diacylglycerol acyltransferase 1-like gene (PtDGAT1) from the diatom *Phaeodactylum tricornutum*. *FEBS J.*, **278**, 3651–3666.

Guindon, S., Dufayard, J.-F.F., Lefort, V., Anisimova, M., Hordijk, W. and Gascuel, O. (2010) New algorithms and methods to estimate maximum-likelihood phylogenies: Asessing the performance of PhyML 2.0. *Syst. Biol.*, **59**, 307–321.

738 **Guo, X., Fan, C., Chen, Y., Wang, J., Yin, W., Wang, R.R.C. and Hu, Z.** (2017)
739 Identification and characterization of an efficient *acyl-CoA: diacylglycerol acyltransferase*
740 *1 (DGAT1)* gene from the microalga *Chlorella ellipsoidea*. *BMC Plant Biol.*, **17**, 48.

741 **Hondred, D., Walker, J.M., Mathews, D.E. and Vierstra, R.D.** (1999) Use of ubiquitin
742 fusions to augment protein expression in transgenic plants. *Plant Physiol.*, **119**, 713–723.

743 **Hu, Q., Sommerfeld, M., Jarvis, E., Ghirardi, M., Posewitz, M., Seibert, M. and Darzins, A.**
744 (2008) Microalgal triacylglycerols as feedstocks for biofuel production: perspectives and
745 advances. *Plant J.*, **54**, 621–639.

746 **Iwai, M., Ikeda, K., Shimojima, M. and Ohta, H.** (2014) Enhancement of extraplastidic oil
747 synthesis in *Chlamydomonas reinhardtii* using a type-2 diacylglycerol acyltransferase with
748 a phosphorus starvation–inducible promoter. *Plant Biotechnol. J.*, **12**, 808–819.

749 **Jacquet, A., Daminet, V., Haumont, M., Garcia, L., Chaudoir, S., Bollen, A. and Biemans,**
750 **R.** (1999) Expression of a recombinant *Toxoplasma gondii* ROP2 fragment as a fusion
751 protein in bacteria circumvents insolubility and proteolytic degradation. *Protein Expr. Purif.*,
752 **17**, 392–400.

753 **Jako, C., Kumar, A., Wei, Y., Zou, J., Barton, D.L., al., et, Giblin, E.M., Covello, P.S. and**
754 **Taylor, D.C.** (2001) Seed-specific over-expression of an Arabidopsis cDNA encoding a
755 diacylglycerol acyltransferase enhances seed oil content and seed weight. *Plant Physiol.*,
756 **126**, 861–874.

757 **Katavic, V., Reed, D.W., Taylor, D.C., Ciblin, E.M., Barton, D.L., Zou, J., Mackenzie, S.L.,**
758 **Covello, P.S. and Kunst, L.** (1995) Alteration of seed fatty acid composition by an ethyl
759 methanesulfonate-induced mutation in *Arabidopsis thaliana* affecting diacylglycerol
760 acyltransferase activity. *Plant Physiol.*, **108**, 399–409.

761 **Katoh, K. and Standley, D.M.** (2013) MAFFT multiple sequence alignment software version 7:
762 Improvements in performance and usability. *Mol. Biol. Evol.*, **30**, 772–780.

763 **Kim, H., Park, J.H., Kim, A.Y., Suh, M.C., Kim, D.J., Kim, Y.A. and Suh, M.C.** (2016)
764 Functional analysis of *diacylglycerol acyltransferase1* genes from *Camelina sativa* and
765 effects of *CsDGAT1B* overexpression on seed mass and storage oil content in *C. sativa*.
766 *Plant Biotechnol. Rep.*, **10**, 141–153.

Kirchner, L., Wirshing, A., Kurt, L., Reinard, T., Glick, J., Cram, E.J., Jacobsen, H.-J. and Lee-Parsons, C.W.T. (2016) Identification, characterization, and expression of diacylgylcerol acyltransferase type-1 from *Chlorella vulgaris*. *Algal Res.*, **13**, 167–181.

Knudsen, J., Faergeman, N.J., Skøtt, H., et al. (1994) Yeast acyl-CoA-binding protein: acyl-CoA-binding affinity and effect on intracellular acyl-CoA pool size. *Biochem. J.*, **302**, 479–485.

Kong, F., Romero, I.T., Warakanont, J. and Li-Beisson, Y. (2018) Lipid catabolism in microalgae. *New Phytol.*, **218**, 1340–1348.

Kremers, G., Goedhart, J., Munster, E.B. Van and Gadella, T.W.J. (2006) Cyan and yellow super fluorescent proteins with improved brightness, protein folding, and FRET Förster radius. *Biochemistry*, **45**, 6570–6580.

Krink-Koutsoubelis, N., Loechner, A.C., Lechner, A., et al. (2018) Engineered poduction of short-chain acyl-Coenzyme A esters in *Saccharomyces cerevisiae*. *ACS Synth. Biol.*, **7**, 1105–1115.

Krogh, A., Larsson, B., Heijne, G. von and Sonnhammer, E. (2001) Predicting transmembrane protein topology with a hidden Markov model: Application to complete genomes. *J. Mol. Biol.*, **305**, 567–580.

Kroon, J.T.M., Wei, W., Simon, W.J. and Slabas, A.R. (2006) Identification and functional expression of a type 2 acyl-CoA:diacylglycerol acyltransferase (DGAT2) in developing castor bean seeds which has high homology to the major triglyceride biosynthetic enzyme of fungi and animals. *Phytochemistry*, **67**, 2541–2549.

Lardizabal, K., Effertz, R., Levering, C., Mai, J., Pedroso, M.C., Jury, T., Aasen, E., Gruys, K. and Bennett, K. (2008) Expression of *Umbelopsis ramanniana DGAT2A* in seed increases oil in soybean. *Plant Physiol.*, **148**, 89–96.

Larson, T.R. and Graham, I. a. (2001) A novel technique for the sensitive quantification of acyl CoA esters from plant tissues. *Plant J.*, **25**, 115–125.

Letunic, I. and Bork, P. (2016) Interactive tree of life (iTOL) v3: An online tool for the display and annotation of phylogenetic and other trees. *Nucleic Acids Res.*, **44**, W242–W245.

Li, R., Yu, K. and Hildebrand, D.F. (2010) *DGAT1*, *DGAT2* and *PDAT* expression in seeds and other tissues of epoxy and hydroxy fatty acid accumulating plants. *Lipids*, **45**, 145–57.

Li, R., Yu, K., Wu, Y., et al. (2012) *Vernonia* DGATs can complement the disrupted oil and protein metabolism in epoxygenase-expressing soybean seeds. *Metab. Eng.*, **14**, 29–38.

Liu, B. and Benning, C. (2013) Lipid metabolism in microalgae distinguishes itself. *Curr Opin Biotechnol*, **24**, 300–309.

Liu, J., Han, D., Yoon, K., Hu, Q. and Li, Y. (2016) Characterization of type 2 diacylglycerol acyltransferases in *Chlamydomonas reinhardtii* reveals their distinct substrate specificities and functions in triacylglycerol biosynthesis. *Plant J.*, **86**, 3–19.

Liu, J., Sun, Z., Mao, X., Gerken, H., Wang, X. and Yang, W. (2019) Multi-omics analysis reveals distinct mechanism of oleaginousness in the emerging model alga Chromochloris zofingiensis. *Plant J.*, **98**, 1060–1077.

Liu, Q., Siloto, R.M.P., Lehner, R., Stone, S.J. and Weselake, R.J. (2012) Acyl-CoA:diacylglycerol acyltransferase: molecular biology, biochemistry and biotechnology. *Prog. Lipid Res.*, **51**, 350–377.

Mandrup, S., Jepsen, R., Skøtt, H., Rosendal, J., Højrup, P., Kristiansen, K. and Knudsen, J. (1993) Effect of heterologous expression of acyl-CoA-binding protein on acyl-CoA level and composition in yeast. *Biochem. J.*, **290**, 369–374.

Mao, X., Wu, T., Kou, Y., Shi, Y., Zhang, Y. and Liu, J. (2019) Characterization of type I and type II diacylglycerol acyltransferases from the emerging model alga *Chlorella zofingiensis* reveals their functional complementarity and engineering potential. *Biotechnol. Biofuels*, **12**, 28.

Marsh, J.A., Stadel, J.M., Ecker, D.J. and Crooke, S.T. (1989) Ubiquitin fusion augments the yield of cloned gene products in *Escherichia coli*. *Proc. Natl. Acad. Sci.*, **86**, 2540–2544.

McFie, P.J., Stone, S.L., Banman, S.L. and Stone, S.J. (2010) Topological orientation of acyl-CoA:diacylglycerol acyltransferase-1 (DGAT1) and identification of a putative active site histidine and the role of the n terminus in dimer/tetramer formation. *J. Biol. Chem.*, **285**, 37377–37387.

Miao, R., Lung, S.-C., Li, X., Li, X.D. and Chye, M.-L. (2019) Thermodynamic insights into an interaction between ACYL-COA-BINDING PROTEIN2 and LYSOPHOSPHOLIPASE2 in *Arabidopsis*. *J. Biol. Chem.*, **294**, 6214–6226.

Mietkiewska, E., Miles, R., Wickramarathna, A., Sahibollah, A.F., Greer, M.S., Chen, G. and Weselake, R.J. (2014) Combined transgenic expression of *Punica granatum* conjugase (*FADX*) and *FAD2* desaturase in high linoleic acid *Arabidopsis thaliana* mutant leads to increased accumulation of punicic acid. *Planta*, **240**, 575–583.

Mishra, S., Yadav, D.K. and Tuli, R. (2006) Ubiquitin fusion enhances cholera toxin B subunit expression in transgenic plants and the plant-expressed protein binds GM1 receptors more efficiently. *J. Biotechnol.*, **127**, 95–108.

Moreno, A.J., Venegas, M., Vaistij, F.E., Salas, J.J., Larson, T.R., Garcés, R., Graham, I.A. and Martínez, E. (2014) Effect of a mutagenized acyl-ACP thioesterase FATA allele from sunflower with improved activity in tobacco leaves and Arabidopsis seeds. *Planta*, **239**, 667–677.

O'Quin, J.B., Mullen, R.T. and Dyer, J.M. (2009) Addition of an N-terminal epitope tag significantly increases the activity of plant fatty acid desaturases expressed in yeast cells. *Appl. Microbiol. Biotechnol.*, **83**, 117–125.

Oakes, J., Brackenridge, D., Colletti, R., et al. (2011) Expression of fungal *diacylglycerol acyltransferase2* genes to increase kernel oil in maize. *Plant Physiol.*, **155**, 1146–1157.

Pryor, K.D. and Leiting, B. (1997) High-level expression of soluble protein in *Escherichia coli* using a His 6 -tag and maltose-binding-protein double-affinity fusion system. *Protein Expr. Purif.*, **10**, 309–319.

Rahman, H., Harwood, J. and Weselake, R. (2013) Increasing seed oil content in Brassica species through breeding and biotechnology. *Lipid Technol.*, **25**, 182–185.

Ro, D., Paradise, E.M., Ouellet, M., et al. (2006) Production of the antimalarial drug precursor artemisinic acid in engineered yeast. *Nature*, **440**, 940–943.

Robinson, C. V, Chung, E.W., Kragelund, B.B., Knudsen, J., Aplin, R.T., Poulsen, F.M. and Dobson, C.M. (1996) Probing the nature of noncovalent interactions by mass spectrometry. A study of protein - CoA ligand binding and assembly. *J. Am. Chem. Soc.*,

118, 8646–8653.

Roesler, K., Shen, B., Bermudez, E., et al. (2016) An improved variant of soybean type 1 diacylglycerol acyltransferase increases the oil content and decreases the soluble carbohydrate content of soybeans. *Plant Physiol.*, **171**, 878–893.

Roth, M.S., Cokus, S.J., Gallaher, S.D., et al. (2017) Chromosome-level genome assembly and transcriptome of the green alga *Chromochloris zofingiensis* illuminates astaxanthin production. *Proc. Natl. Acad. Sci. U. S. A.*, **114**, E4296–E4305.

Sandager, L., Gustavsson, M.H., Stahl, U., Dahlqvist, A., Wiberg, E., Banas, A., Lenman, M., Ronne, H. and Stymne, S. (2002) Storage lipid synthesis is non-essential in yeast. *J Biol Chem*, **277**, 6478–6482.

Schjerling, C.K., Hummel, R., Hansen, J.K., Børsting, C., Mikkelsen, J.M., Kristiansen, R. and Knudsen, J. (1996) Disruption of the gene encoding the acyl-CoA-binding protein (ACB1) perturbs acyl-CoA metabolism in Saccharomyces cerevisiae. *J. Biol. Chem.*, **271**, 22514–22521.

Schneider, C.A., Rasband, W.S. and Eliceiri, K.W. (2012) NIH Image to ImageJ: 25 years of image analysis. *Nat. Methods*, **9**, 671–675.

Shockey, J.M., Gidda, S.K., Chapital, D.C., Kuan, J.-C.C., Dhanoa, P.K., Bland, J.M., Rothstein, S.J., Mullen, R.T. and Dyer, J.M. (2006) Tung tree DGAT1 and DGAT2 have nonredundant functions in triacylglycerol biosynthesis and are localized to different subdomains of the endoplasmic reticulum. *Plant Cell*, **18**, 2294–2313.

Siloto, R.M.P., Madhavji, M., Wiehler, W.B., Burton, T.L., Boora, P.S., Laroche, A. and Weselake, R.J. (2008) An N-terminal fragment of mouse DGAT1 binds different acyl-CoAs with varying affinity. *Biochem. Biophys. Res. Commun.*, **373**, 350–354.

Singer, S.D., Chen, G., Mietkiewska, E., Tomasi, P., Jayawardhane, K., Dyer, J.M. and Weselake, R.J. (2016) Arabidopsis GPAT9 contributes to synthesis of intracellular glycerolipids but not surface lipids. *J. Exp. Bot.*, **67**, 4627–4638.

Sriram, S.M., Kim, B.Y. and Kwon, Y.T. (2011) The N-end rule pathway: Emerging functions and molecular principles of substrate recognition. *Nat. Rev. Mol. Cell Biol.*, **12**, 735–747.

Streatfield, S.J. (2007) Approaches to achieve high-level heterologous protein production in plants. *Plant Biotechnol. J.*, **5**, 2–15.

Tian, L. and Sun, S.S.M. (2011) Ubiquitin fusion expression and tissue-dependent targeting of hG-CSF in transgenic tobacco. *BMC Biotechnol.*, **11**, 91.

Turchetto-Zolet, A.C., Maraschin, F.S., Morais, G.L. De, Cagliari, A., Andrade, C.M., Margis-Pinheiro, M. and Margis, R. (2011) Evolutionary view of acyl-CoA diacylglycerol acyltransferase (DGAT), a key enzyme in neutral lipid biosynthesis. *BMC Evol. Biol.*, **11**, 263.

Tzen, J., Cao, Y., Laurent, P., Ratnayake, C. and Huang, A. (1993) Lipids, proteins, and structure of seed oil bodies from diverse species. *Plant Physiol.*, **101**, 267–276.

Vanhercke, T., Divi, U.K., Tahchy, A. El, et al. (2017) Step changes in leaf oil accumulation via iterative metabolic engineering. *Metab. Eng.*, **39**, 237–246.

Vanhercke, T., Tahchy, A. El, Shrestha, P., Zhou, X.-R.R., Singh, S.P. and Petrie, J.R. (2013) Synergistic effect of WRI1 and DGAT1 coexpression on triacylglycerol biosynthesis in plants. *FEBS Lett.*, **587**, 364–9.

Ward, J.J., McGuffin, L.J., Bryson, K., Buxton, B.F. and Jones, D.T. (2004) The DISOPRED server for the prediction of protein disorder. *Bioinformatics*, **20**, 2138–2139.

Wei, H., Shi, Y., Ma, X., Pan, Y., Hu, H., Li, Y., Luo, M., Gerken, H. and Liu, J. (2017) A type-I diacylglycerol acyltransferase modulates triacylglycerol biosynthesis and fatty acid composition in the oleaginous microalga, *Nannochloropsis oceanica*. *Biotechnol. Biofuels*, **10**, 174.

Weselake, R.J., Madhavji, M., Szarka, S.J., et al. (2006) Acyl-CoA-binding and self-associating properties of a recombinant 13.3 kDa N-terminal fragment of diacylglycerol acyltransferase-1 from oilseed rape. *BMC Biochem.*, **7**, 24.

Weselake, R.J., Pomeroy, M.K., Furukawa, T.L., Golden, J.L., Little, D.B. and Laroche, A. (1993) Developmental profile of diacylglycerol acyltransferase in maturing seeds of oilseed rape and safflower and microspore-derived cultures of oilseed rape. *Plant Physiol.*, **102**, 565–571.

Weselake, R.J., Shah, S., Tang, M., et al. (2008) Metabolic control analysis is helpful for informed genetic manipulation of oilseed rape (*Brassica napus*) to increase seed oil content. *J. Exp. Bot.*, **59**, 3543–3549.

Xin, Y., Lu, Y., Lee, Y.-Y.Y., et al. (2017) Producing designer oils in industrial microalgae by rational modulation of co-evolving type-2 diacylglycerol acyltransferases. *Mol. Plant*, **10**, 1523–1539.

Xin, Y., Shen, C., She, Y., et al. (2018) Biosynthesis of triacylglycerol molecules with tailored PUFA profile in industrial microalgae. *Mol. Plant*.

Xu, Y., Caldo, K.M.P., Pal-Nath, D., Ozga, J., Lemieux, M.J., Weselake, R.J. and Chen, G. (2018) Properties and biotechnological applications of acyl-CoA:diacylglycerol acyltransferase and phospholipid:diacylglycerol acyltransferase from terrestrial plants and microalgae. *Lipids*, **53**, 663–688.

Xu, Y., Chen, G., Greer, M.S., et al. (2017) Multiple mechanisms contribute to increased neutral lipid accumulation in yeast producing recombinant variants of plant diacylglycerol acyltransferase 1. *J. Biol. Chem.*, **292**, 17819–17831.

Xu, Y., Falarz, L. and Chen, G. (2019) Characterization of type-2 diacylglycerol acyltransferases in the green microalga *Chromochloris zofingiensis*. *J. Agric. Food Chem.*, **67**, 291–298.

Xu, Y., Holic, R., Li, D., Pan, X., Mietkiewska, E., Chen, G., Ozga, J., Weselake, R.J. and Holic, R. (2018) Substrate preferences of long-chain acyl-CoA synthetase and diacylglycerol acyltransferase contribute to enrichment of flax seed oil with α-linolenic acid. *Biochem. J.*, **475**, 1473–1489.

Yurchenko, O.P., Nykiforuk, C.L., Moloney, M.M., Ståhl, U., Banaś, A., Stymne, S. and Weselake, R.J. (2009) A 10-kDa acyl-CoA-binding protein (ACBP) from *Brassica napus* enhances acyl exchange between acyl-CoA and phosphatidylcholine. *Plant Biotechnol. J.*, **7**, 602–610.

Yurchenko, O.P. and Weselake, R.J. (2011) Involvement of low molecular mass soluble acyl-CoA-binding protein in seed oil biosynthesis. *N. Biotechnol.*, **28**, 97–109.

Zou, J., Wei, Y., Jako, C., Kumar, A., Selvaraj, G. and Taylor, D.C. (1999) The *Arabidopsis*

thaliana TAG1 mutant has a mutation in a diacylglycerol acyltransferase gene. *Plant J.*, **19**, 645–653.

Zulu, N.N., Popko, J., Zienkiewicz, K., Tarazona, P., Herrfurth, C. and Feussner, I. (2017) Heterologous co-expression of a yeast diacylglycerol acyltransferase (ScDGA1) and a plant oleosin (AtOLEO3) as an efficient tool for enhancing triacylglycerol accumulation in the marine diatom *Phaeodactylum tricornutum*. *Biotechnol. Biofuels*, **10**, 187.

945 **TABLES**

946

947 **Table 1. Apparent kinetic parameters of CzDGAT1 variants.** DGAT activity was examined
948 at increasing oleoyl-CoA concentration from 0.1 to 7.5 or 10 μM. Data were fitted to a nonlinear
949 regression using allosteric sigmoidal equation with GraphPad Prism software. Data shown are
950 means ± S.D. (n=3).

951

Enzyme	$DGAT1_{1-550}$	$DGAT1_{81-550}$	ACBP-$DGAT1_{1-550}$	ACBP-$DGAT1_{81-550}$
Apparent V_{max} (pmol TAG/min/mg protein)	276.8±6.94	17.14±0.28	436.7±10.1	34.54±1.27
Hill coefficient	1.39±0.06	1.71±0.06	1.91±0.12	1.57±0.14
Apparent $S_{0.5}$ (μM)	1.48±0.07	1.83±0.05	0.94±0.04	1.50±0.10
Goodness of Fit/R^2	0.994	0.995	0.981	0.973

952

953

954 **FIGURE LEGENDS**

955 **Figure 1. Phylogenetic relationship among CzDGAT1 and DGAT1 from other organisms.**
956 The organism and Phytozome/GenBank accession number/JGI protein ID for each protein
957 sequence are shown as follows: *Auxenochlorella protothecoides*, *Ap*, ApDGAT1
958 (XP_011402032); *Arabidopsis thaliana*, *At*, AtDGAT1 (NM_127503); *Brassica napus*, *Bn*,
959 BnDGAT1 (JN224473); *Bos taurus*, *Bt*, BtDGAT1 (AAL49962); *Caenorhabditis elegans*, *Cae*,
960 CaeDGAT1 (NM_001269372); *Chlorella ellipsoidea*, *Che*, CheDGAT1 (KT779429);
961 *Chlamydomonas reinhardtii*, *Cre*, CreDGAT1 (Cre01.g045903); *Camelina sativa*, *Cs*,
962 CsDGAT1 (XM_010417066); *Coccomyxa subellipsoidea* C-169, *Csu*, CsuDGAT1 (54084);
963 *Chlorella vulgaris*, *Cv*, CvDGAT1 (ALP13863); *Chromochloris zofingiensis*, *Cz*, CzDGAT1A
964 (MH523419), CzDGAT1B (Cz09g08290); *Drosophila melanogaster*, *Dm*, DmDGAT1
965 (AF468649); *Danio rerio*, *Dr*, DrDGAT1 (NM_199730); *Euonymus alatus*, *Ea*, EaDGAT1
966 (AY751297); *Glycine max*, *Gm*, GmDGAT1 (AY496439); *Helianthus annuus*, *Ha*, HaDGAT1
967 (HM015632); *Homo sapiens*, *Hs*, HsDGAT1 (NM_012079); *Jatropha curcas*, *Jc*, JcDGAT1
968 (DQ278448); *Klebsormidium nitens*, *Kn*, KnDGAT1 (GAQ91878); *Linum usitatissimum*, *Lu*,
969 LuDGAT1 (KC485337); *Monodelphis domestica*, *Md*, MdDGAT1 (XM_007488766); *Mus*
970 *musculus*, *Mm*, MmDGAT1 (AF078752); *Medicago truncatula*, *Mt*, MtDGAT1
971 (XM_003595183); *Nannochloropsis oceanica*, *No*, NoDGAT1 (KY073295); *Nicotiana tabacum*,
972 *Nt*, NtDGAT1 (AF129003); *Nematostella vectensis*, *Nv*, NvDGAT1 (XM_001639301); *Olea*
973 *europae*, *Oe*, OeDGAT1 (AY445635); *Oryza sativa*, *Os*, OsDGAT1 (NM_001061404);
974 *Paracoccidioides brasiliensis*, *Pb*, PbDGAT1 (EEH17170); *Perilla frutescens*, *Pf*, PfDGAT1
975 (AF298815); *Populus trichocarpa*, *Pot*, PotDGAT1 (XM_006371934); *Physcomitrella patens*,
976 *Pp*, PpDGAT1 (XM_001770877); *Phaeodactylum tricornutum*, *Pt*, PtDGAT1 (HQ589265);
977 *Ricinus communis*, *Rc*, RcDGAT1 (NM_001323734); *Rattus norvegicus*, *Rn*, RnDGAT1
978 (AB062759); *Sesamum indicum*, *Si*, SiDGAT1 (JF499689); *Sus scrofa*, *Ss*, SsDGAT1
979 (NM_214051); *Trichoplax adhaerens*, *Ta*, TaDGAT1 (XM_002111989); *Toxoplasma gondii*, *Tg*,
980 TgDGAT1 (AY327327); *Tropaeolum majus*, *Tm*, TmDGAT1 (AY084052); *Thalassiosira*
981 *pseudonana*, *Tp*, TpDGAT1 (XM_002287179); *Vernicia fordii*, *Vf*, VfDGAT1 (DQ356680);
982 *Vernonia galamensis*, *Vg*, VgDGAT1 (EF653276); *Vitis vinifera*, *Vv*, VvDGAT1 (CAN80418);
983 *Yarrowia lipolytica*, *Yl*, YlDGAT1 (XM_502557); and *Zea mays*, *Zm*, ZmDGAT1 (EU039830).
984 DGAT1s from the animal, fungal, green algal, and plant groups are shown in orange, blue, pink

and green, respectively. Algal DGAT1s are shown by red bars. The length of the N-terminus of DGAT1 is shown as a heat map (circle).

Figure 2. CzDGAT1 encodes an active enzyme and has a unique N-terminus with less propensity to become disordered. A and B, Triacylglycerol (TAG) content (A) and fatty acid (FA) composition (B) in yeast producing CzDGAT1 cultured in the absence of FA or the presence of exogenous linoleic acid (18:2$\Delta^{9cis,12cis}$, 18:2), or α-linolenic acid (C18:3$\Delta^{9cis,12cis,15cis}$, 18:3). Yeast cells were harvested after 48 h of induction for lipid analysis. C16:0, Palmitic acid; C18:0, Stearic acid; C18:1, Oleic acid. C, *In vitro* DGAT assay using yeast microsomal fractions containing recombinant CzDGAT1. D, Sequence alignment of the N-terminal regions of DGAT1. *At*, *Arabidopsis thaliana*; *Bn*, *Brassica napus*; *Cv*, *Chlorella vulgaris*; *Cz*, *Chromochloris zofingiensis*; *No*, *Nannochloropsis oceanica*. E and F, Prediction of intrinsic disorder profile (blue) of the N-terminal regions of CzDGAT1 (D) and BnDGAT1 (E) and likelihood to participate in protein-protein interaction (red) by DISOPRED analysis (Ward *et al.*, 2004). For A, B and C, data represent means ± S.D. (n = 3).

Figure 3. Truncation analysis of the N-terminal domain CzDGAT1. A, Predicted topology of CzDGAT1 by TMHMM (Krogh *et al.*, 2001). CzDGAT1 has a 107-amino acid residue-long hydrophilic N-terminal region, followed by 9 predicted transmembrane domains (TMDs). The numbers indicate the different truncation points. B, Protein production level of the full-length ($CzDGAT1_{1-550}$) and N-terminal truncated ($CzDGAT1_{81-550}$ and $CzDGAT1_{107-550}$) CzDGAT1 variant proteins. The enzyme amount was semi-quantified by Image J software (Schneider *et al.*, 2012). C, *In vitro* DGAT activity of $CzDGAT1_{1-550}$, $CzDGAT1_{81-550}$ or $CzDGAT1_{107-550}$. D, Normalized DGAT activity of $CzDGAT1_{1-550}$, $CzDGAT1_{81-550}$ or $CzDGAT1_{107-550}$. Normalized activity was calculated by dividing the activity value by the corresponding protein accumulation. Data represent means ± S.D. (n = 3).

Figure 4. N-terminal fusion of an acyl-CoA binding protein (ACBP) with CzDGAT1 and its N-terminal truncation mutants. A, Protein production level of the full-length CzDGAT1

(DGAT1$_{1-550}$), N-terminal truncated CzDGAT1 (DGAT1$_{81-550}$ and DGAT1$_{107-550}$) and their corresponding ACBP fused proteins (ACBP-DGAT1$_{1-550}$, ACBP-DGAT1$_{81-550}$ and ACBP-DGAT1$_{107-550}$). The enzyme amount was semi-quantified by Image J software (Schneider *et al.*, 2012). B, *In vitro* DGAT activity of the full-length, N-terminal truncated and ACBP fused CzDGAT1 proteins. C, Normalized DGAT activity of the full-length, N-terminal truncated and ACBP fused CzDGAT1 proteins. Normalized activity was calculated by dividing the activity value by the corresponding protein accumulation. Data represent means ± S.D. (n = 3).

Figure 5. N-terminal fusion of an acyl-CoA binding protein (ACBP) with CzDGAT1 kinetically improves the enzyme. A-D, DGAT activities of the full-length CzDGAT1 (DGAT1$_{1-550}$), N-terminal truncated CzDGAT1 (DGAT1$_{81-550}$) and their corresponding ACBP fused proteins (ACBP-DGAT1$_{1-550}$ and ACBP-DGAT1$_{81-550}$) at oleoyl-CoA concentration from 0.1-7.5 or 10 μM. Data were fitted to the allosteric sigmoidal equation using GraphPad Prism. Data represent means ± S.D. (n = 3).

Figure 6. Fusion of acyl-CoA binding protein (ACBP) with CzDGAT1 boosts oil production in yeast and *Nicotiana benthamiana* leaves. A, Neutral lipid accumulation in yeast production ACBP-fused DGAT1. B, Triacylglycerol (TAG) content in transiently transformed *N. benthamiana* leaves. All cDNAs were constitutively expressed under the *CaMV 35S* promoter with the co-expression of the *p19* vector and *Arabidopsis thaliana Wrinkled1* (*AtWRI1*). C, Fatty acid composition of TAG in in transiently transformed *N. benthamiana* leaves. D, Subcellular localization of ACBP-fused DGAT1 in *N. benthamiana* leaf cells. Venus-tagged DGAT1 or ACBP-DGAT1 was co-localized with C-terminal SCFP3A tagged *Arabidopsis thaliana* glycerol-3-phosphate acyltransferase (AtGPAT9), a known endoplasmic reticulum (ER) localized protein. Scale bars represent 20 μm. E, Fluorescence intensity of ACBP-fused DGAT1. *N. benthamiana* leaves transiently expressing *Venus-DGAT1* or *Venus-ACBP-DGAT1* and the *p19* vector were used to quantify the fluorescent intensity. F, Western-blot immunodetection detection against V5 tagged ACBP-fused DGAT1 or DGAT1 on *N. benthamiana* leaf proteins. Coomassie Blue staining of duplicate leaf protein samples separated on SDS-PAGE gel is shown as a loading control. G, Relative protein accumulation levels of ACBP-fused DGAT1 or DGAT1

in *N. benthamiana* leaf cells based on western blot analysis. The enzyme amount was semi-quantified by Image J software (Schneider *et al.*, 2012). C16:0, Palmitic acid; C18:0, Stearic acid; C18:1, Oleic acid; C18:2, Linoleic acid; C18:3, α-linolenic acid; p19, p19 + AtWRI1; $DGAT1_{1-550}$, p19 + AtWRI1 + $CzDGAT1_{1-550}$; ACBP-$DGAT1_{1-550}$, p19 + AtWRI1 + ACBP fused $CzDGAT1_{1-550}$; ACBP+$DGAT1_{1-550}$, p19 + AtWRI1 + ACBP + $CzDGAT1_{1-550}$; $DGAT1_{81-550}$, p19 + AtWRI1 + $CzDGAT1_{81-550}$; ACBP-$DGAT1_{81-550}$, p19 + AtWRI1 + ACBP fused $CzDGAT1_{81-550}$; ACBP+$DGAT1_{81-550}$, p19 + AtWRI1 + ACBP + $CzDGAT1_{81-550}$. Data represent means ± S.D. For A and G, n=3; for B and C, n=7; for E, n=4. The asterisk and pound sign indicate $P < 0.05$ as determined by paired one-tailed T-test.

Fig.1

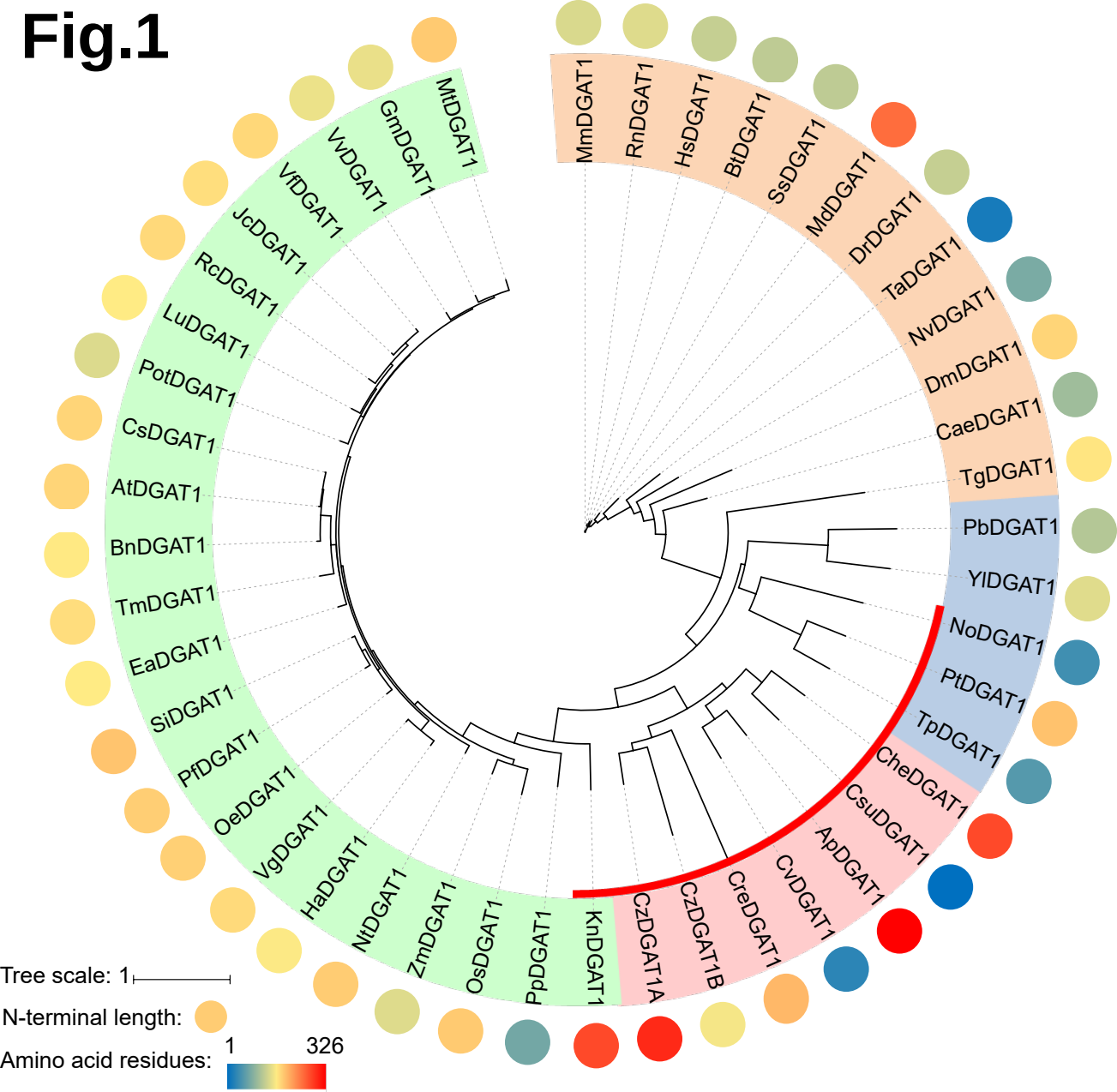
MtDGAT1
GmDGAT1
VvDGAT1
VfDGAT1
JcDGAT1
RcDGAT1
LuDGAT1
PotDGAT1
CsDGAT1
AtDGAT1
BnDGAT1
TmDGAT1
EaDGAT1
SiDGAT1
PfDGAT1
OeDGAT1
VgDGAT1
HaDGAT1
NtDGAT1
ZmDGAT1
OsDGAT1
PpDGAT1
KnDGAT1
CzDGAT1A
CzDGAT1B
CreDGAT1
CvDGAT1
ApDGAT1
CsuDGAT1
CheDGAT1
TpDGAT1
PtDGAT1
NoDGAT1
YlDGAT1
PbDGAT1
TgDGAT1
CaeDGAT1
DmDGAT1
NvDGAT1
TaDGAT1
DrDGAT1
MdDGAT1
SsDGAT1
BtDGAT1
HsDGAT1
RnDGAT1
MmDGAT1
Tree scale: 1
N-terminal length:
Amino acid residues:
1
326

Fig.2

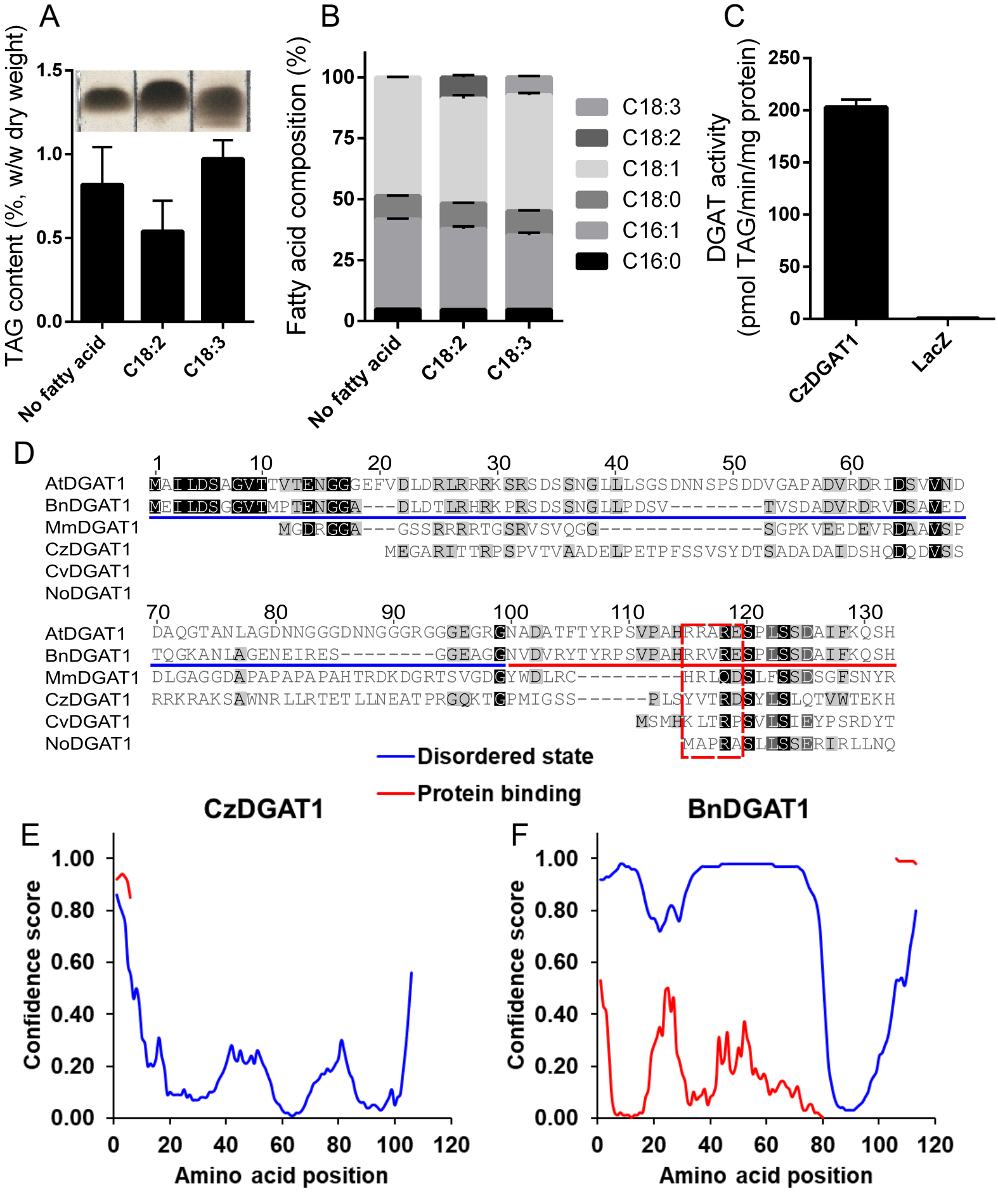

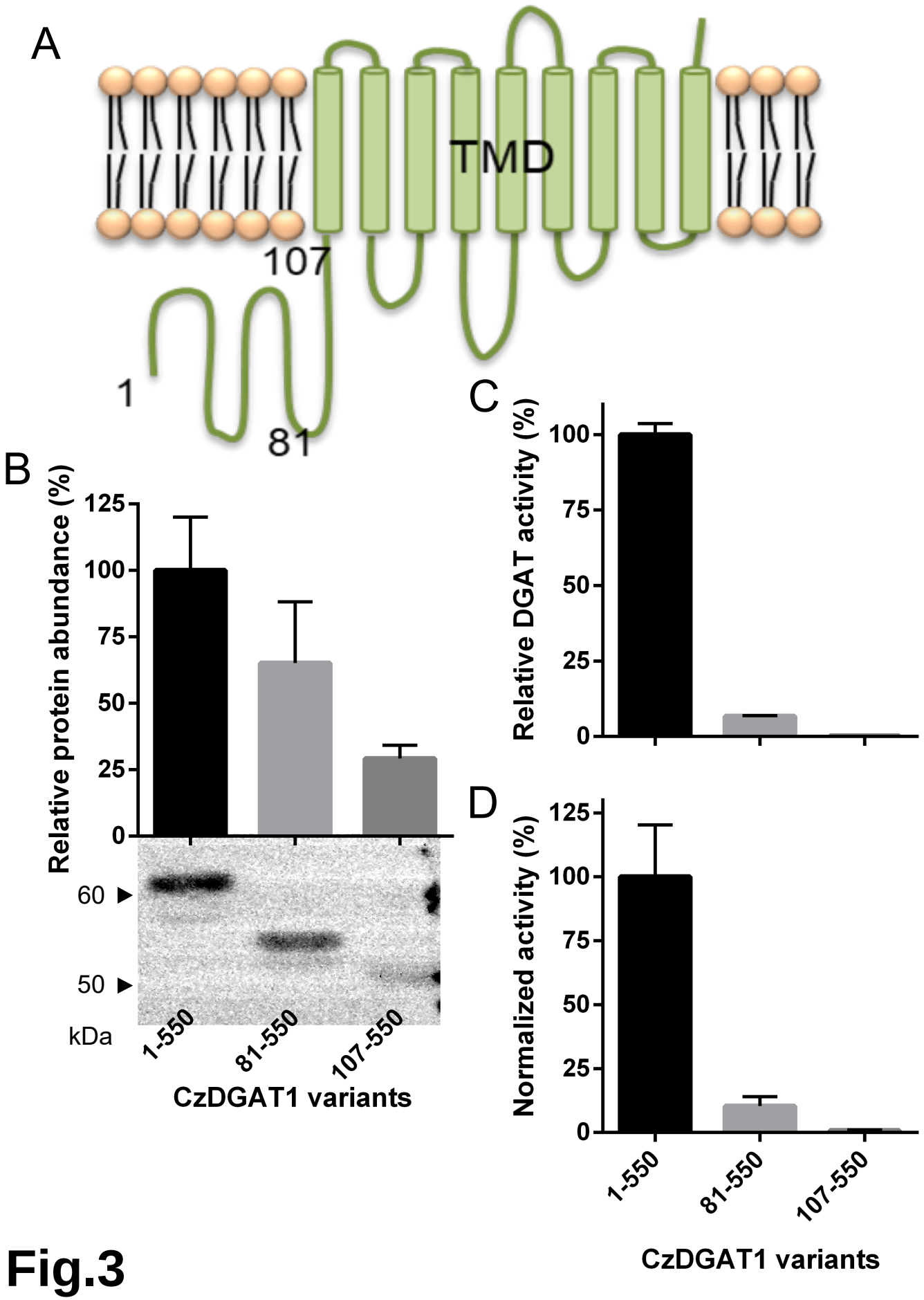

Fig.3

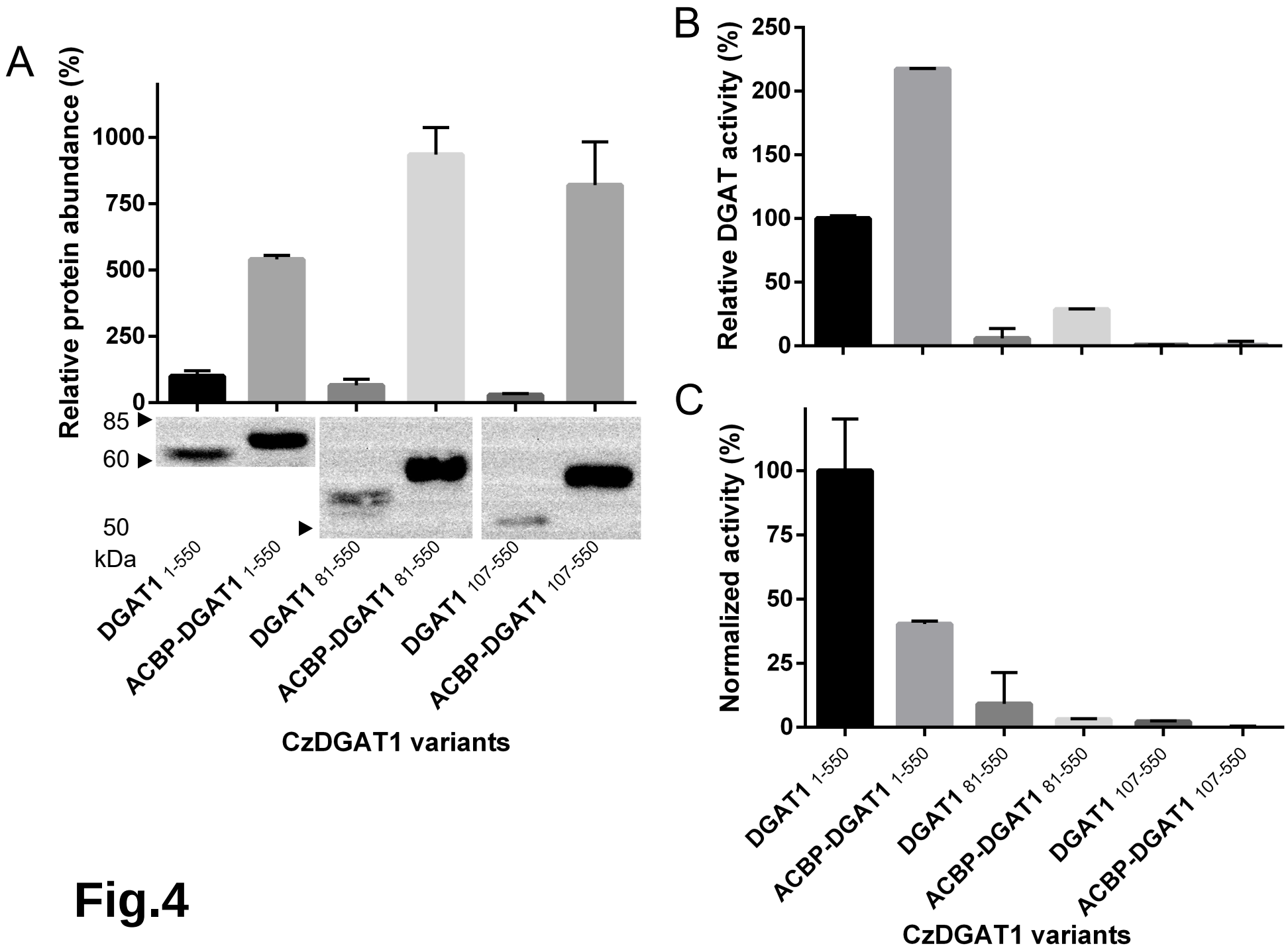
A
Relative protein abundance (%)
1000
750
500
250
0
85
60
50
kDa
DGAT1 1-550
ACBP-DGAT1 1-550
DGAT1 81-550
ACBP-DGAT1 81-550
DGAT1 107-550
ACBP-DGAT1 107-550
CzDGAT1 variants
B
Relative DGAT activity (%)
250
200
150
100
50
0
C
Normalized activity (%)
100
75
50
25
0
DGAT1 1-550
ACBP-DGAT1 1-550
DGAT1 81-550
ACBP-DGAT1 81-550
DGAT1 107-550
ACBP-DGAT1 107-550
CzDGAT1 variants

Fig.4

Fig.5

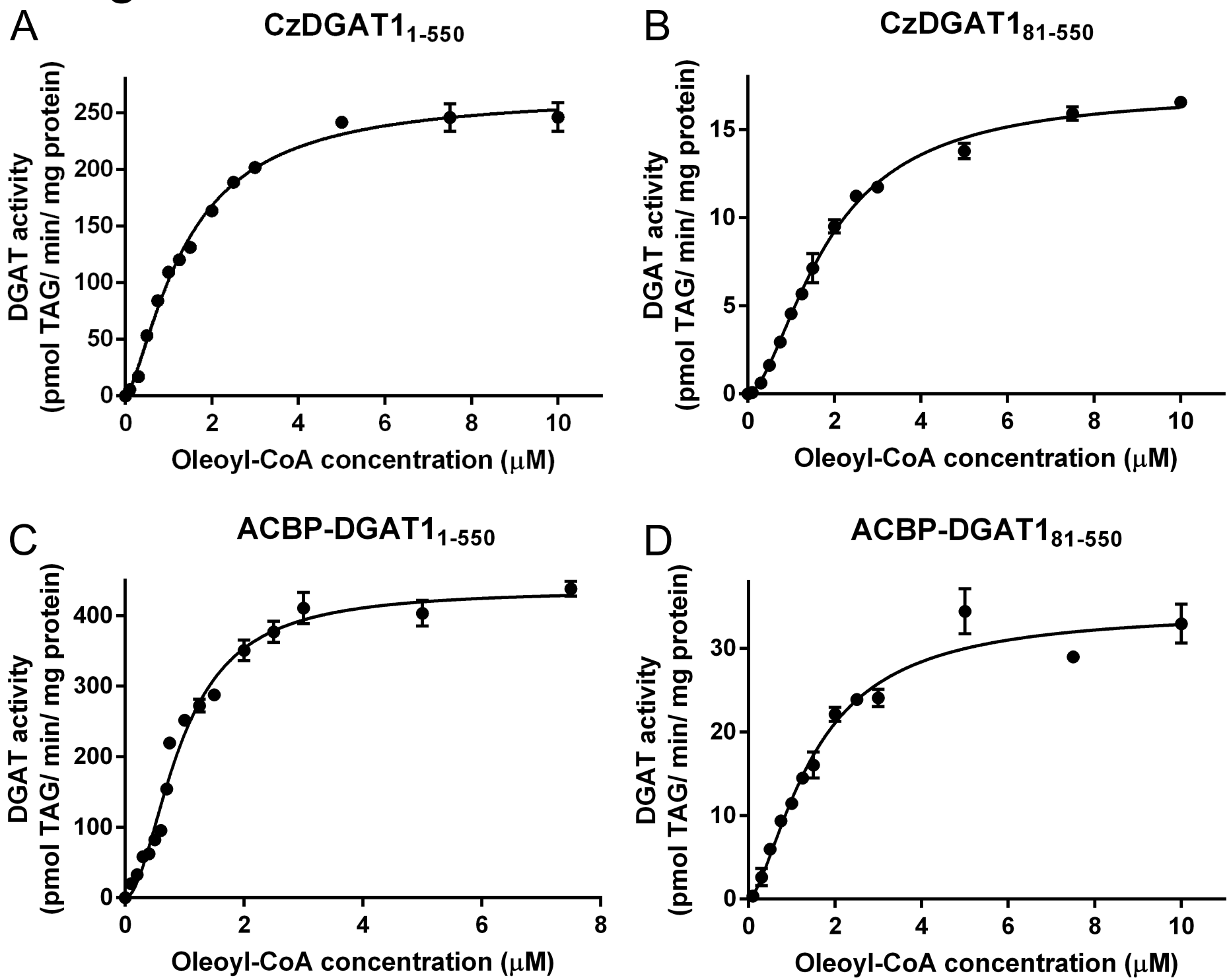
A
CzDGAT1$_{1-550}$
DGAT activity
(pmol TAG/ min/ mg protein)
0
50
100
150
200
250
0
2
4
6
8
10
Oleoyl-CoA concentration (μM)
B
CzDGAT1$_{81-550}$
DGAT activity
(pmol TAG/ min/ mg protein)
0
5
10
15
0
2
4
6
8
10
Oleoyl-CoA concentration (μM)
C
ACBP-DGAT1$_{1-550}$
DGAT activity
(pmol TAG/ min/ mg protein)
0
100
200
300
400
0
2
4
6
8
Oleoyl-CoA concentration (μM)
D
ACBP-DGAT1$_{81-550}$
DGAT activity
(pmol TAG/ min/ mg protein)
0
10
20
30
0
2
4
6
8
10
Oleoyl-CoA concentration (μM)

Fig.6

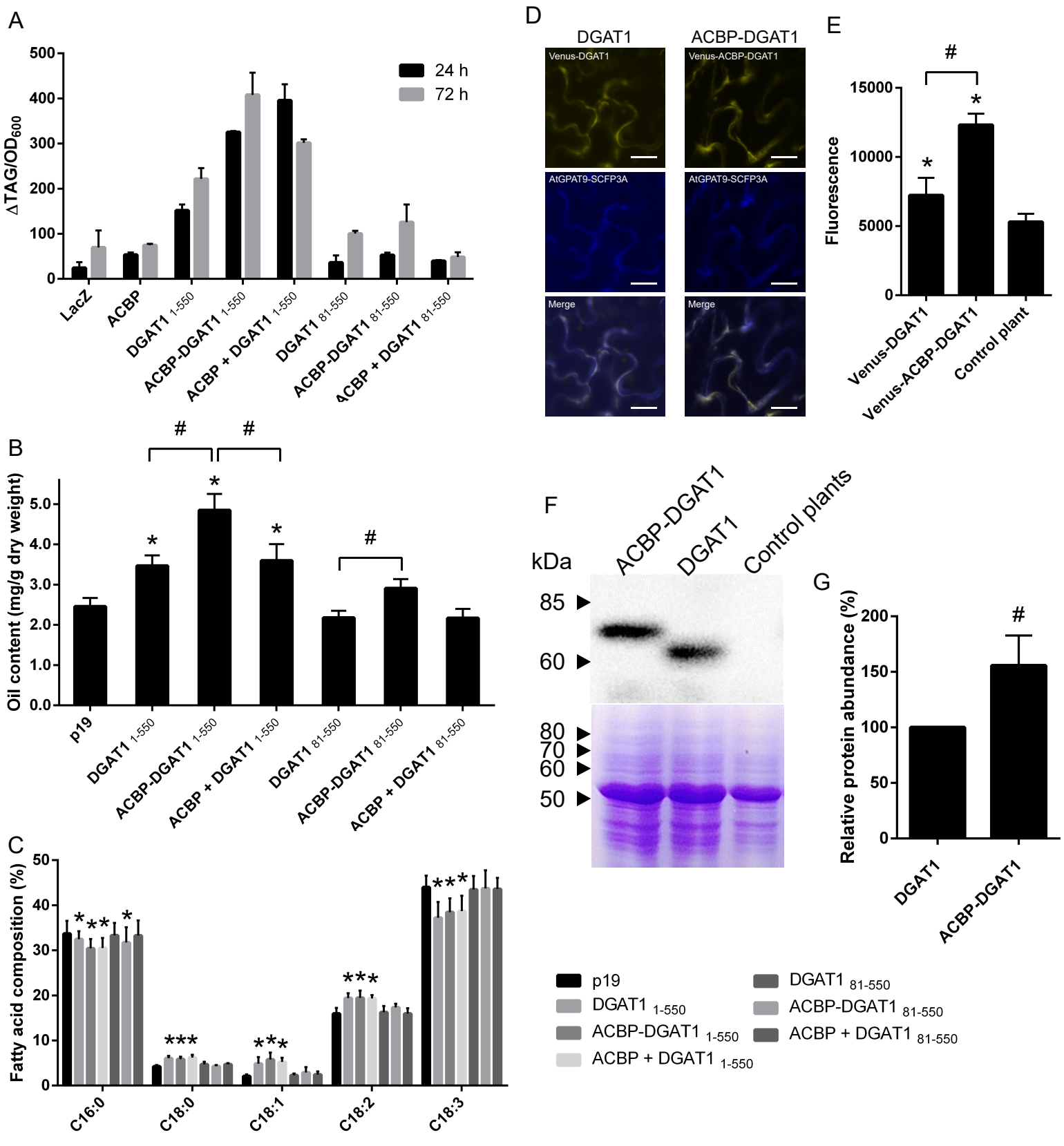
A
ΔTAG/OD600
24 h
72 h
LacZ
ACBP
DGAT1 1-550
ACBP-DGAT1 1-550
ACBP + DGAT1 1-550
DGAT1 81-550
ACBP-DGAT1 81-550
ACBP + DGAT1 81-550
B
Oil content (mg/g dry weight)
p19
C
Fatty acid composition (%)
C16:0
C18:0
C18:1
C18:2
C18:3
D
DGAT1
ACBP-DGAT1
Venus-DGAT1
Venus-ACBP-DGAT1
AtGPAT9-SCFP3A
Merge
E
Fluorescence
Venus-DGAT1
Venus-ACBP-DGAT1
Control plant
F
kDa
ACBP-DGAT1
DGAT1
Control plants
85
60
80
70
60
50
G
Relative protein abundance (%)
DGAT1
ACBP-DGAT1
p19
DGAT1 1-550
ACBP-DGAT1 1-550
ACBP + DGAT1 1-550
DGAT1 81-550
ACBP-DGAT1 81-550
ACBP + DGAT1 81-550